

Parallelly Tempered Generative Adversarial Networks

Jinwon Sohn

Department of Statistics, Purdue University

and

Qifan Song

Department of Statistics, Purdue University

Abstract

A generative adversarial network (GAN) has been a representative backbone model in generative artificial intelligence (AI) because of its powerful performance in capturing intricate data-generating processes. However, the GAN training is well-known for its notorious training instability, usually characterized by the occurrence of mode collapse. Through the lens of gradients' variance, this work particularly analyzes the training instability and inefficiency in the presence of mode collapse by linking it to multimodality in the target distribution. To ease the raised training issues from severe multimodality, we introduce a novel GAN training framework that leverages a series of tempered distributions produced via convex interpolation. With our newly developed GAN objective function, the generator can learn all the tempered distributions simultaneously, conceptually resonating with the parallel tempering in Statistics. Our simulation studies demonstrate the superiority of our approach over existing popular training strategies in both image and tabular data synthesis. We theoretically analyze that such significant improvement can arise from reducing the variance of gradient estimates by using the tempered distributions. Finally, we further develop a variant of the proposed framework aimed at generating fair synthetic data which is one of the growing interests in the field of trustworthy AI.

Keywords: Generative Adversarial Network, Parallel Tempering, Fair Data Generation, Variance Reduction

1 Introduction

The rising demand for bigger data with privacy has led to the widespread adoption of data generators (or synthesizers) across various domains (Jordon et al., 2022). For instance, the European General Data Protection Regulation mandates data deletion after its primary purpose and restricts sharing due to ownership and privacy concerns. As a promising solution, Mottini et al. (2018) employed a generative model to synthesize Passenger-Name-Records (PNR) data while discarding the original one to comply with such a data protection policy. Meanwhile, large-scale AI models, devouring massive training datasets, exploit the generative model’s capability to produce an arbitrary number of data points for efficient training (Hwang et al., 2023). In the literature, the generative adversarial network (GAN, Goodfellow et al., 2014) particularly stands out as a versatile data synthesizer, demonstrating exceptional capabilities in reconstructing diverse datasets, such as images (Kang et al., 2023), text (de Rosa and Papa, 2021), tabular data (Zhao et al., 2021), and even estimating model parameters (Wang and Ročková, 2022).

The GAN framework consists of two competing networks $D \in \mathcal{D}$ (i.e., the critic) and $G \in \mathcal{G}$ (i.e., the generator) where \mathcal{D} and \mathcal{G} have neural-net families. Let $X \in \mathcal{X} = \mathbb{R}^{d_X}$ and $Z \in \mathcal{Z} = \mathbb{R}^{d_Z}$ be random variables with density p_X and p_Z respectively. We denote by $G : \mathbb{R}^{d_Z} \rightarrow \mathbb{R}^{d_X}$ the generator that ideally transforms the reference variable Z to be $G(Z) \stackrel{d}{=} X$. The essence of learning (or estimating) G starts from approximating a divergence $d(p_X, p_{G(Z)})$ between two probability distributions by \mathcal{D} , i.e., $d(p_X, p_{G(Z)}) \approx d_{\mathcal{D}}(p_X, p_{G(Z)})$. Then it finds the optimal G satisfying $d_{\mathcal{D}}(p_X, p_{G(Z)}) = 0$. Under this general framework, diverse probability metrics have been attempted such as the Jensen-Shannon divergence (JSD, Goodfellow et al., 2014), the 1-Wasserstein distance (Arjovsky et al., 2017), f -divergence (Nowozin et al., 2016), and so forth.

Despite its great potential as a high-quality data synthesizer, GAN has been known to be brutally unstable and easily fall into nonconvergence because of its min-max (or adversarial) optimization structure. To resolve this training issue, there has been a plethora of research discovering better training tricks or network architectures, mostly based on empirical findings and specifically for image data synthesis (Jabbar et al., 2021). From a more fundamental perspective, Mescheder et al. (2018) suggested penalizing the average gradient norm of D , so that there would be no power to break the equilibrium between D and G . Zhou et al. (2019) discussed that unstable training may arise from the flow of meaningless gradients from D to G , which is resolved by enforcing \mathcal{D} to be Lipschitz. To see more relevant studies, refer to Roth et al. (2017); Gulrajani et al. (2017).

Tempering (or smoothing) p_X has also been studied as an effective strategy to stabilize the GAN training mainly for the information-based divergence. Arjovsky and Bottou (2017) theoretically justified that the JSD-based GAN training with some random noise being annealed $\epsilon \rightarrow 0$ during training, i.e., $\min_G d_{\mathcal{D}}(p_{X+\epsilon}, p_{G(Z)+\epsilon})$, can improve optimization. They show that expanding supports of X and $G(Z)$ by adding ϵ can enable D and G to yield meaningful and stabilized gradients. Based on this notable study, Sajjadi et al. (2018) attempted annealing a functional noise of X created by an auxiliary neural network during the GAN training with JSD. Jenni and Favaro (2019) approached $\min_G d_{\mathcal{D}}(p_{X+\epsilon}, p_{G(Z)+\epsilon})$ with JSD where a noise ϵ is learned by an extra network instead of following an annealing schedule.

While the existing studies benefit from resolving the unstable optimization issue of JSD associated with support mismatch, this work discovers a stable training mechanism by tempering a multimodal p_X via a convex interpolation scheme in GAN with the approximated 1-Wasserstein distance. Based on this novel discovery of smoothing p_X in GAN training,

we eventually devise an efficient and stable GAN framework by learning multiple levels of tempered distributions simultaneously, so it is called the parallelly tempered generative adversarial networks (PTGAN). Section 2 explains the estimation mechanism of the GAN training and discusses a source of training instability focusing on characterizing the gradients’ variance of the critic. Section 3 defines the convex interpolation that creates a tempered density of p_X and analyzes how it alleviates the multimodality of p_X . Section 4 specifically designs the proposed framework that effectively incorporates the interpolation scheme without an annealing schedule. While our approach inherently possesses a bias-variance trade-off in updating the critic, the learned GAN model achieves the nearly optimal minimax rate. Lastly, Section 5 verifies that PTGAN significantly outperforms popular competing models in various benchmark data sets. Moreover, we extend PTGAN for a fair data generation task to which trustworthy AI has paid great attention recently. To our knowledge, this is the first work to theoretically analyze the GAN mechanism through the lens of the gradients’ variance of D with the tempered density of p_X .

2 Estimation Mechanism of GAN

2.1 Neural distance

To define a target distance metric $d_{\mathcal{D}}$, let’s consider families of fully-connected neural networks: $\mathcal{D} = \{D(x) = w_d^\top \kappa_{d-1}(W_{d-1} \kappa_{d-2}(\cdots W_1 x)) : \mathbf{w} = (W_1, \dots, W_{d-1}, w_d) \in \mathbf{W}\}$ and $\mathcal{G} = \{G(z) = v_g^\top \psi_{g-1}(V_{g-1} \psi_{g-2}(\cdots V_1 z)) : \mathbf{v} = (V_1, \dots, V_{g-1}, v_g) \in \mathbf{V}\}$, where $w_d \in \mathbb{R}^{p_d \times 1}$, $v_d \in \mathbb{R}^{q_d \times d_X}$, $W_i \in \mathbb{R}^{p_{i+1} \times p_i}$ for $i = 1, \dots, d-1$, $V_j \in \mathbb{R}^{q_{j+1} \times q_j}$ for $j = 1, \dots, g-1$, $p_1 = d_X$, and $q_1 = d_Z$; κ_i and ψ_j are element-wise non-linear activation functions. Then the neural distance (Arora et al., 2017) is defined as follows.

Definition 1. Let $X \sim p_X$ and $Z \sim p_Z$. For a given monotone concave function $\phi : \mathbb{R} \rightarrow \mathbb{R}$, $G \in \mathcal{G}$, and $D \in \mathcal{D}$, $d_{\mathcal{D}}(p_X, p_{G(Z)}) = \sup_{D \in \mathcal{D}} \mathbf{E}(\phi(D(X))) + \mathbf{E}(\phi(1 - D(G(Z))))$ is called a neural distance between X and $G(Z)$.

The specification of ϕ determines the type of discrepancy. With $\phi(x) = \log(x)$ and the sigmoid output of D , $d_{\mathcal{D}}$ approximates JSD. If $\phi(x) = x$, the 1-Wasserstein distance is approximated via the Kantorovich-Rubinstein duality. This work particularly focuses on the identity mapping of ϕ , which leads to the approximated 1-Wasserstein distance by D :

$$d_{\mathcal{D}}(p_X, p_{G(Z)}) = \sup_{D \in \mathcal{D}} \mathbf{E}(D(X)) - \mathbf{E}(D(G(Z))). \quad (1)$$

For this target distance, the optimal critic function D^* is the maximizer of $L(D, G) = \mathbf{E}(D(X)) - \mathbf{E}(D(G(Z)))$ such that $d_{\mathcal{D}}(p_X, p_{G(Z)}) = \mathbf{E}(D^*(X)) - \mathbf{E}(D^*(G(Z)))$, and the optimal generator G^* is the minimizer of $d_{\mathcal{D}}(p_X, p_{G^*(Z)})$. For theoretical analysis in the remaining sections, the following assumptions are made:

(A1) Bounded parameter: $\mathbf{W} = \bigotimes_{i=1}^{d-1} \{W_i \in \mathbb{R}^{p_{i+1} \times p_i} : \|W_i\|_F \leq M_w(i)\} \otimes \{w_d \in \mathbb{R}^{p_d \times 1} : \|w_d\| \leq M_w(d)\}$ and $\mathbf{V} = \bigotimes_{j=1}^{g-1} \{V_j \in \mathbb{R}^{q_{j+1} \times q_j} : \|V_j\|_F \leq M_v(j)\} \otimes \{v_g \in \mathbb{R}^{q_g \times d} : \|v_g\| \leq M_v(g)\}$ with constants $M_w(\cdot)$ and $M_v(\cdot)$. Note $\|\cdot\|_F$ and $\|\cdot\|$ denote the Frobenius and the Euclidean norm respectively.

(A2) Lipschitz activation: κ_i and ψ_j are $K_{\kappa}(i)$ - and $K_{\psi}(j)$ -Lipschitz functions for all i, j , i.e., $\|\psi_j(x) - \psi_j(y)\| \leq K_{\psi}(j)\|x - y\|$ for any $x, y \in \mathbb{R}$, and also for κ_i as well.

(A3) Bounded support: $\mathcal{X} \subset \{\|x\| \leq B_X, x \in \mathbb{R}^{d_X}\}$ and $\mathcal{Z} \subset \{\|z\| \leq B_Z, z \in \mathbb{R}^{d_Z}\}$.

These assumptions can be readily satisfied. For (A1), ad-hoc training techniques such as weight clipping or weight normalization (Miyato et al., 2018) can be used. For (A2), popular activation functions such as Relu, Leaky Relu (lRelu), Sigmoid, and Tanh are 1-Lipschitz.

Finally, for (A3), it is common to normalize the input variable in the deep learning literature, e.g., $-1 \leq X \leq 1$ (a.k.a. min-max normalization), and place a uniform distribution to Z .

2.2 Adversarial estimation

2.2.1 Iterative gradient-based estimation from minibatches

Let's denote by X_1, \dots, X_n and Z_1, \dots, Z_m the i.i.d. samples drawn from p_X and p_Z respectively. We define $\mathbf{X}_{1:n} = \{X_1, \dots, X_n\}$. Since p_X is unknown in general and D and G can be highly nonlinear, the min-max optimization relies on the iterative gradient-based estimation with an empirical estimator of L . We particularly employ $\hat{L}_b(D, G) = \sum_{i=1}^{n_b} D(X_i)/n_b - \sum_{j=1}^{m_b} D(G(Z_j))/m_b$ where, with a slight abuse of notation, $\{X_1, \dots, X_{n_b}\}$ denotes a minibatch randomly chosen from $\mathbf{X}_{1:n}$ with $n_b, m_b \ll n$. For feasible computation, most modern machine learning models adopt such a minibatch scheme for training.

To estimate D^* and G^* , the iterative gradient-based estimation alternates gradient ascent/descent at the t th iteration, i.e.,

$$\mathbf{w}^{(t+1)} = \mathbf{w}^{(t)} + \gamma_D \frac{\partial}{\partial \mathbf{w}^{(t)}} \hat{L}_b(D^{(t)}, G^{(t)}), \quad \mathbf{v}^{(t+1)} = \mathbf{v}^{(t)} - \gamma_G \frac{\partial}{\partial \mathbf{v}^{(t)}} \hat{L}_b(D^{(t+1)}, G^{(t)}), \quad (2)$$

where $D^{(t)}$ and $G^{(t)}$ (or $\mathbf{w}^{(t)}$ and $\mathbf{v}^{(t)}$) are the t th iterate of D and G , and γ_D and γ_G are learning rates. Throughout this paper, $D^{(t)}$ and $G^{(t)}$ are also denoted as $\mathbf{w}^{(t)}$ and $\mathbf{v}^{(t)}$ according to the context respectively. For simplicity, m_b is set to be equal to n_b .

2.2.2 Estimation dynamics

To describe the estimation behavior, we denote \mathcal{S} as the high-density support region of X , such that the probability density of p_X out of \mathcal{S} is reasonably small. In the extreme case, we may directly consider that \mathcal{X} is a disconnected set (with each disconnected component representing a mode of p_X) and $\mathcal{S} = \mathcal{X}$. To characterize the distribution modes

learned by $G^{(t)}$ (i.e., a subset of \mathcal{S}), we define the recovered support of p_X by $G^{(t)}$ as $\mathcal{S}_t = \mathcal{S} \cap \{G^{(t)}(z), z \in \mathcal{Z}\}$, and $\mathcal{S}_t^c = \mathcal{S} \setminus \mathcal{S}_t$ the remaining support which is missing by $G^{(t)}$. Unless \mathcal{S} is fully recovered, we say that the estimand $G^{(t)}$ for G^* is incomplete. For ease of later discussion, we denote $p_{\mathcal{S}_t}$ and $p_{\mathcal{S}_t^c}$ as normalized probability density functions of p_X restricted on \mathcal{S}_t and \mathcal{S}_t^c respectively, meaning $p_{\mathcal{S}_t}$ represents the recovered distribution components of the target p_X by $G^{(t)}$.

When $G^{(t)}$ has such incomplete support recovery, $D^{(t)} \rightarrow D^{(t+1)}$ is necessarily updated by either maximizing $\sum_{i=1}^{n_b} D^{(t)}(X_i)/n_b$ or minimizing $\sum_{i=1}^{m_b} D^{(t)}(G^{(t)}(Z_i))/m_b$. This opposite directional optimization encourages $D^{(t+1)}$ to assign higher values to X_i and lower values to $G^{(t)}(Z_i)$, so $D^{(t+1)}$ appropriately identifies the discrepancy between the support of $G^{(t)}(Z)$ and \mathcal{S}_t^c by its value. The desirable $D^{(t+1)}$ then guides the direction and size of the generator’s gradients for the update of $G^{(t)} \rightarrow G^{(t+1)}$ such that $G^{(t+1)}$ accounts for more areas in \mathcal{S} . More specifically, for $z \in \mathcal{Z}$, the gradient of $\mathbf{v}^{(t)}$ with respect to \hat{L}_b is $\partial \hat{L}_b / \partial \mathbf{v}^{(t)} = - [\nabla_g D^{(t+1)}(g)]_{g=G^{(t)}(z)} \cdot \partial G^{(t)}(z) / \partial \mathbf{v}^{(t)}$. The gradient component $\nabla_g D^{(t+1)}(g)$ instructs the update of $G^{(t)}$ so that $G^{(t+1)}$ properly accounts for the support having higher $D^{(t+1)}$ values (likely in \mathcal{S}_t^c if $D^{(t+1)}$ successfully characterizes the gap between $G^{(t)}(Z)$ and \mathcal{S}_t^c). In this regard, accurate estimation for the neural distance (or equivalently $\mathbf{w}^{(t+1)}$) is of great importance. In an ideal situation, the generator eventually fully recovers \mathcal{S} after a sufficient number of iterations T , i.e., $\mathcal{S}_T \approx \mathcal{S}$, reaching out the approximate equilibrium $L(D', G^{(T)}) \lesssim L(D^{(T)}, G^{(T)}) \lesssim L(D^{(T)}, G')$ for any $D' \in \mathcal{D}$ and $G' \in \mathcal{G}$. Therefore, $G^{(T)}$ is regarded as an empirical estimator \hat{G}^* for G^* .

Unfortunately, this adversarial process tends to easily forget some of the captured areas in $\mathcal{S}_{t'}$ at a later $t(> t')$ th iteration particularly when p_X is multimodal. For a toy example in Figure 1, the generator revolves around unimodal distributions. This *mode collapse*

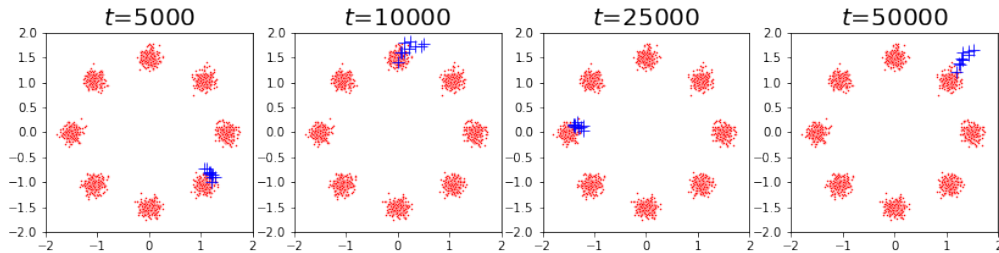


Figure 1: Mode collapse behavior: target distribution (plain dots) and $G^{(t)}(Z)$ (cross dots). Each unimodal distribution is 1.5 away from the origin and has a variance of 0.01. For \mathcal{D} and \mathcal{G} , $p_{i+1} = q_{i+1} = 256$ and $\kappa_i(x) = \max\{x, 0\}$ (Relu) for $i = 1, \dots, d - 1$ (and $g - 1$ respectively) where $d = g = 5$ and $d_Z = 4$. Both n_b and m_b are set to be 100.

behavior is a persistent challenge in GAN literature. In the literature, Goodfellow (2017) suggested that the conventional update scheme (2) may inadvertently address a max-min problem, which encourages the generator to produce only the most probable modes with the highest values. An et al. (2020) claimed that the continuity of the generator by neural networks may be fundamentally incompatible when the underlying distribution p_X consists of disconnected components, contributing to mode collapse. To mitigate mode collapse, various studies have been proposed in the literature (Zhou et al., 2019; Kim et al., 2023). The exact cause of mode collapse, however, still remains unknown.

2.3 Inefficient estimation under severe multimodality

This section explores how mode collapse worsens GAN training by focusing on the behavior of gradients' variance of D w.r.t. the discrepancy between $G^{(t)}$ and \mathcal{S}_t^c . To our knowledge, this perspective as a way of understanding the GAN mechanism has not yet been attempted in the literature. Our analysis begins by observing mode collapse gives rise to multimodality between $G^{(t)}$ and \mathcal{S}_t^c . Keeping in mind this relationship, we first demonstrate that the neural distance is a well-suited metric for assessing multimodality, and then clarify that the

degree of multimodality is closely associated with the size of gradients' variance.

2.3.1 Assessing the degree of multimodality

In Statistics, p_X is called a multimodal distribution when its density function has more than one peak. For example, p_X that consists of two unimodal distributions p_k for $k = 1, 2$ whose mean and variance are μ_k and σ_k^2 shapes a bimodal density expressed by $p_X(x) = \sum_{k=1}^2 p_k(x; \mu_k, \sigma_k^2)/2$. To simplify a discussion, we suppose $\sigma = \sigma_1 = \sigma_2$. As a way of measuring bimodality of p_X , one can come up with the ratio of between-variability and within-variability like $|\mu_1 - \mu_2|/\sigma$ (Ashman et al., 1994; Wang et al., 2009). Likewise, the neural distance represents the degree of bimodality as shown in the following Proposition 1, but it mainly reflects the between-variability when equal variances are given.

Proposition 1. Under (A1-3), the neural distance between probability distributions $p_1(x; \mu_1, \sigma^2)$ and $p_2(x; \mu_2, \sigma^2)$ in a location-scale distribution family is bounded by

$$|\mu_1 - \mu_2| - \delta_{\mathcal{D}} \leq d_{\mathcal{D}}(p_1, p_2) \leq \min \left\{ \prod_{l=1}^d M_w(l) \prod_{s=1}^{d-1} K_{\kappa}(s) |\mu_1 - \mu_2|, |\mu_1 - \mu_2| + \delta_{\mathcal{D}} \right\},$$

where $\delta_{\mathcal{D}}$ stands for the universal approximation capability of \mathcal{D} , i.e., the neural networks in \mathcal{D} can approximate any 1-Lipschitz function with $\delta_{\mathcal{D}}$ error on a compact support (please refer to Supplementary B.1 for a more concrete explanation of $\delta_{\mathcal{D}}$).

Note that the between-variability becomes equal to the classic bimodality if the data points are scaled such as x/σ . Although the proposition is written for the specific univariate family of p_1 and p_2 , it is reasonable to posit that the neural distance generally expresses the degree of *multimodality* between any distinguishable distributions p_1 and p_2 . That is, the larger value of $d_{\mathcal{D}}(p_1, p_2)$ intuitively implies that p_X is exposed to substantial multimodality.

2.3.2 Inflation of gradients' variance under mode collapse

Such characterization of multimodality by the neural distance is the key step to examine the GAN training mechanism (2) under the presence of mode collapse. That is, we say that $d_{\mathcal{D}}(p_{\mathcal{S}_t^c}, p_{G^{(t)}})$ signifies the degree of multimodality in mode collapse. Here, we show that severe multimodality induced by incomplete $G^{(t)}$ can cause the GAN training process to be statistically inefficient or unstable, by investigating the gradients' variance of $D^{(t)}$. This analysis ultimately justifies that the use of tempered distributions of p_X can remarkably improve GAN training.

At first, we derive a lower bound of the gradients' variance of $D^{(t)}$. Due to its highly nonlinear structure, we particularly focus on the last weight matrix $w_d^{(t)}$, but $W_k^{(t)}$, for $k = 1, \dots, d-1$, are expected to show the similar tendency due to the connectivity of $W_k^{(t)}$ to $w_d^{(t)}$ via backpropagation. As the first step, we design a classification rule in terms of the t th loss function. Let $L_i^{(t)} = D^{(t)}(X_i) - \mathbf{E}[D^{(t)}(G^{(t)}(Z))]$ for the i th entity. Then, as shown in Figure 2 with the 2-mixture p_X with $\sigma^2 = 0.01$, $\mathbf{E}(L_i^{(t)} | L_i^{(t)} \geq \epsilon)$ implicitly stands for the remaining distance $d_{\mathcal{D}}(p_{\mathcal{S}_t^c}, p_{G^{(t)}})$ for some small ϵ , which allows for explaining the below lower bound by the neural distance. The details of Figure 2 appear in Supplementary D.1.

Proposition 2. Assume $\|w_d^{(t)}\| > 0$. Let $\delta_t^\epsilon = P(L_i^{(t)} \leq \epsilon)$, $\sigma_{\mathcal{S}_t}^2 = \text{Var}(L_i^{(t)} | L_i^{(t)} \leq \epsilon)$, and $\sigma_{G^{(t)}}^2 = \text{Var}(D^{(t)}(G^{(t)}(Z_j)))$. If $\mathbf{E}(L_i^{(t)} | L_i^{(t)} \leq \epsilon) = 0$ for some $\epsilon > 0$, the norm of the covariance of the w_d 's gradient is bounded below by

$$\left\| \text{Cov} \left(\frac{\partial \hat{L}_b(D^{(t)}, G^{(t)})}{\partial w_d^{(t)}} \right) \right\|_2 \geq \frac{\delta_t^\epsilon \sigma_{\mathcal{S}_t}^2 + \delta_t^\epsilon (1 - \delta_t^\epsilon) \mathbf{E}(L_i^{(t)} | L_i^{(t)} \geq \epsilon)^2 + \sigma_{G^{(t)}}^2}{n_b \|w_d^{(t)}\|^2}, \quad (3)$$

where $\|\cdot\|_2$ for the covariance matrix is the induced 2-norm.

Proposition 2 implies that the gradient update of $w_d^{(t)}$ becomes more noisy (hence the estimation of the neural distance becomes statistically inefficient) as $G^{(t)}$ and \mathcal{S}_t^c get

more distant (such as mode collapse), which eventually leads to unstable and inefficient GAN training. From this perspective, we say that *the GAN training for p_X with severe multimodality is essentially much harder than with less multimodality*. As empirical evidence in Figure 2, the case of $\mu_2 = 3.0$, which has larger multimodality, involves a much larger gradient variance.

Next, an upper bound of the gradients' variance of $D^{(t)}$ is derived. To simplify notation, let's denote by $W_{k,i,j}^{(t)}$ the (i, j) th parameter of $W_k^{(t)}$ for $k = 1, \dots, d$; the second index of $W_{d,i,j}^{(t)}$ is regarded dummy for $w_d^{(t)}$, i.e., $w_{d,j}^{(t)} = W_{d,i,j}^{(t)}$. We also define a technical constant reflecting backpropagation in the analysis; $C_{w,\kappa}(k) = \prod_{l=k+1}^d \sqrt{p_l} M_w^{(t)}(l) \prod_{s=k}^{d-1} K_\kappa(s)$ for $k = 1, \dots, d-2$, $C_{w,\kappa}(d-1) = M_w(d)K_\kappa(d-1)$, and $C_{w,\kappa}(d) = 1$.

Theorem 1. Under (A1-3), the size of gradients is bounded above by

$$\left| \frac{\partial \hat{L}_b(D^{(t)}, G^{(t)})}{\partial W_{k,i,j}^{(t)}} \right| \leq C_{w,\kappa}(k) d_{\mathcal{D}}(p_X, p_{G^{(t)}(Z)}) + O_p\left(\frac{1}{\sqrt{n_b}}\right), \quad (4)$$

for $k = 1, \dots, d$.

The square of the upper bound in (4) becomes the bounds for gradients' variance since $\text{Var}(X) \leq \mathbf{E}(X^2)$. Moreover, because $p_X(x) = \delta_t p_{\mathcal{S}_t}(x) + (1 - \delta_t) p_{\mathcal{S}_t^c}(x)$ for all $x \in \mathcal{S}$ where δ_t is the proportion of the recovered support, we see $d_{\mathcal{D}}(p_X, p_{G^{(t)}(Z)}) \leq \delta_t d_{\mathcal{D}}(p_{\mathcal{S}_t}, p_{G^{(t)}(Z)}) + (1 - \delta_t) d_{\mathcal{D}}(p_{\mathcal{S}_t^c}, p_{G^{(t)}(Z)})$. With this relation, therefore, the upper bound (4) relates to the degree of mode collapse or multimodality of p_X that is rephrased by $d_{\mathcal{D}}(p_{\mathcal{S}_t}, p_{G^{(t)}(Z)})$. Note that under mode collapse, $d_{\mathcal{D}}(p_{\mathcal{S}_t}, p_{G^{(t)}(Z)})$ is generally negligible compared with $d_{\mathcal{D}}(p_{\mathcal{S}_t^c}, p_{G^{(t)}(Z)})$. There can be situations where $d_{\mathcal{D}}(p_{\mathcal{S}_t}, p_{G^{(t)}(Z)})$ is not ignorable, such as when $G^{(t)}$ generates synthetic samples out of \mathcal{S} . In any case, the incomplete training of $G^{(t)}$ may cause the inefficient estimation of the gradients because of the enlarged remaining distance.

The derived bounds above provide some insights to stabilize the general GAN training. Basically, (3) hints that the norm of the weight parameters should not decay faster than

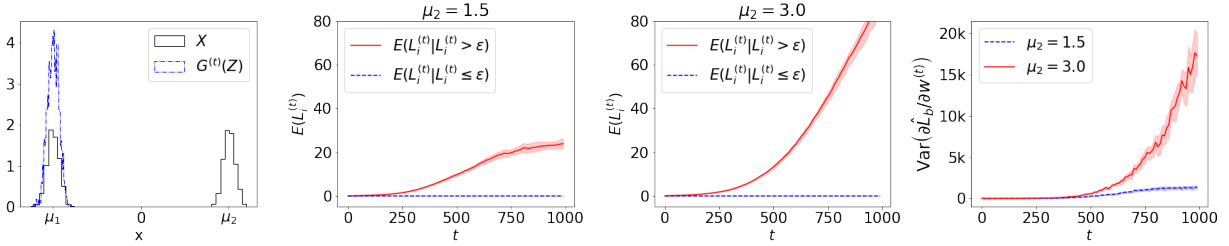


Figure 2: Mode collapse induces multimodality. The leftmost depicts mode collapse where $\mu_1 = -\mu_2$. In all t , $D^{(t)}$ is updated but $G^{(t)}$ is fixed to generate the left mode. The same \mathcal{D} in drawing Figure 1 is used. The middle two panels illustrate the values of $\mathbf{E}(L_i^{(t)})$ along iterations when $\mu_2 = 1.5$ and $\mu_2 = 3.0$ respectively. The rightmost draws the behavior of the gradient variance for each case.

$d_{\mathcal{D}}(p_{S_i^c}, p_{G^{(t)}})$ during the training so that the variance of the gradients does not inflate. Although allowing for large $M_w^{(t)}(l)$ in \mathcal{D} may settle this issue, the bound in (4) becomes too large, which potentially causes unstable training. Hence, it is desirable to have a reasonable $M_w^{(t)}(l)$ during the training, so that the gradients' variance does not inflate or shrink too much as the depth of D gets deeper. This nontrivial observation justifies why the popular training tricks, such as normalizing weight matrices (Miyato et al., 2018) or imposing a penalty on D (Mescheder et al., 2018; Zhou et al., 2019), are practically able to stabilize the adversarial optimization to some extent. Also, our argument supports encouraging a good initialization of $G^{(t)}$ (Zhao et al., 2023) because in general $d_{\mathcal{D}}(p_{S_i^c}, p_{G^{(0)}})$ is likely to be huge. *Moreover, the bounds rationalize that the gradient estimates can enjoy variance reduction effects if it is possible to intrinsically lower $d_{\mathcal{D}}(p_{S_i^c}, p_{G^{(t)}})$ with the norm of weight matrices controlled during the training.*

3 Tempered Distributions via Convex Interpolation

In the previous section, we discussed how mode collapse leads to inefficient training of $D^{(t)}$. In the statistical literature, a similar phenomenon, i.e. the local trapping problem, occurs in the Bayesian sampling of multimodal posterior distributions (Neal, 1996; Liang et al., 2014). To overcome this local trapping issue, a statistical annealing strategy creates a population of sampling targets with changing levels of multimodality, associated with different temperatures. The same idea behind statistical annealing is also expected to be effective for GAN training as well because the tempered distributions of p_X would involve smaller $d_{\mathcal{D}}(p_{S_t^c}, p_{G^{(t)}})$ even though mode collapse occurs. Since the probability density function is generally not accessible in GAN, we implicitly define tempered distributions via a simple idea of the convex mixture.

3.1 Convex interpolation between data points

To temper the unknown p_X , we define an auxiliary random variable that represents a tempered (or intermediate) distribution. The i th weighted random variable Q_i^α is defined as

$$Q_i^\alpha = \alpha X_{i_1} + (1 - \alpha) X_{i_2}, \quad (5)$$

where X_{i_1}, X_{i_2} are two random elements in $\mathbf{X}_{1:n}$ and $0 \leq \alpha \leq 1$. The density of Q_i^α is denoted by p_{Q^α} on support \mathcal{Q} whose size is bounded by $\|\mathcal{Q}^\alpha\| \leq B_X$ as well. Figure 3 illustrates the distribution of Q^α where X follows the 2- and 8-component mixture distribution respectively with $\alpha \sim \text{Unif}(0, 1)$. Evidently, Q^α has a more tempered distribution than X for any α because *the created convex bridge connecting every pair of modes significantly reduces multimodality*. Based on this construction of Q^α , we postulate \mathcal{P}_{Q^α} as the family of tempered densities p_{Q^α} originated from p_X , i.e., $\mathcal{P}_{Q^\alpha} = \{p_{Q^\alpha} : 0 \leq \alpha \leq 1\}$. A similar interpolation

idea was attempted by the Mixup approach (Zhang et al., 2018) in which linear combinations of X_i and $G(Z_i)$ are considered for GAN training. The Mixup strategy, however, only applies to a specific type of $d_{\mathcal{D}}$, whereas ours is universally applicable to most probability metrics. Supplementary A.2 provides an in-depth discussion advocating our approach that interpolates two real samples for GAN training.

3.2 Reduction of multimodality

To figure out how the smoothing mechanism (5) reduces multimodality more concretely, let's consider the 2-mixture example discussed in Section 2.3.1, i.e., $p_X(x) = \sum_{k=1}^2 p_k(x; \mu_k, \sigma)/2$. Pivoting on $X_1 \sim p_1$, Q_1^α is either $\alpha X_1 + (1 - \alpha)X_2$ or $\alpha X_1 + (1 - \alpha)Y_2$ with the same probabilities where $X_2 \sim p_1$ and $Y_2 \sim p_2$ independently. Then we can write the density of Q_1^α as $p_{Q_1^\alpha}(x) = \sum_{k=1}^2 p_k^\alpha(x; \mu_k^*, \sigma^*)/2$ where each p_k^α is specified based on the allocation of X_2 and Y_2 . For instance, p_1^α is defined as the density of $\alpha X_1 + (1 - \alpha)X_2$ while p_2^α corresponds to $\alpha X_1 + (1 - \alpha)Y_2$. In this case, we obtain $|\mu_1^* - \mu_2^*| = (1 - \alpha)|\mu_1 - \mu_2|$ and $\sigma^* = \sqrt{(2\alpha^2 - 2\alpha + 1)\sigma^2}$, so, by Proposition 1, the bimodality perceived by the neural distance tends to diminish for $0 < \alpha < 1$ with consideration of $Q_1^\alpha \stackrel{d}{=} Q_1^{1-\alpha}$. In addition, the classic bimodality decreases as well since $|\mu_1^* - \mu_2^*|/\sigma^* = e(\alpha) \times |\mu_1 - \mu_2|/\sigma$ where $e(\alpha) = \sqrt{(1 - \alpha)^2 / ((1 - \alpha)^2 + \alpha^2)} \leq 1$. The same argument straightforwardly holds as well when Q_1^α pivots on $Y_1 \sim p(x; \mu_2, \sigma)$, i.e., $Q_1^\alpha = \alpha Y_1 + (1 - \alpha)Y_2$ or $Q_1^\alpha = \alpha Y_1 + (1 - \alpha)X_2$ with the same probabilities. Note that there can be other ways to define the mixture components p_1^α and p_2^α but in general the same conclusion is induced.

The above example helps differentiate the convex interpolation from adding a random noise ϵ to X (Arjovsky and Bottou, 2017) in terms of the mechanism to ease multimodality. In essence, simply adding noise may not effectively decrease the multimodality in view

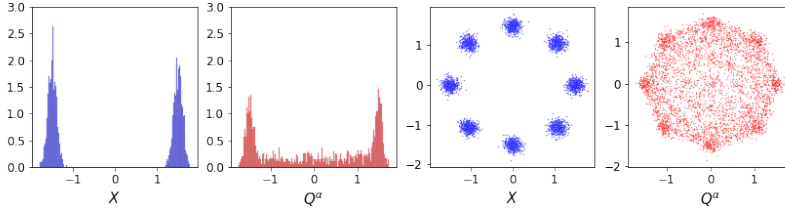


Figure 3: Tempered distributions of p_X : the first and third panels depict histograms of X , with 2- and 8-component mixtures respectively, and the next of each represents Q^α .

of the neural distance because it just increases the within-variability. On the other hand, the convex interpolation not only expands the support of X but also directly lessens the between-variability by building bridges connecting separate local modes. We name this particular property as *mode connectivity*. As anticipated, the distributions in \mathcal{P}_{Q^α} tend to have a higher degree of multimodality if α is close to either 0 or 1 but smaller than p_X if $\alpha \approx 1/2$. Although our argument is made on the simple toy example, it is reasonable to uphold the same argument even when p_X has more underlying unimodal distributions in higher dimensions because the essence of creating Q^α underpins whether or not the interpolated variables connect pairs of disconnected distributions in p_X . For these reasons, we emphasize that *training with Q^α would be likely to have a smaller remaining neural distance $d_{\mathcal{D}}(p_{S_t^\epsilon}, p_{G(t)})$ than training with only X or $X + \epsilon$ when the generator is incomplete.* In such a case, therefore, the training with Q^α would be more stable than with X or $X + \epsilon$ because it tends to have a smaller gradients' variance, as discussed in Section 2.3.2.

4 Parallel Estimation

To leverage tempered distributions p_{Q^α} for eventually learning p_X in GAN training, we refer to a well-known strategy reminiscent of *parallel tempering* in the Bayesian sampling literature (Geyer, 1991; Deng et al., 2023). Our GAN model concurrently learns all distributions

in \mathcal{P}_{Q^α} . In contrast to the previous works relying on annealing strategies (Arjovsky and Bottou, 2017; Sajjadi et al., 2018) or finding a specific temperature (Jenni and Favaro, 2019), our framework does not rely on either of these techniques.

4.1 Joint optimization with randomized temperature

The proposed parallel tempering framework is designed to estimate a series of generators for all intermediate distributions in \mathcal{P}_{Q^α} simultaneously. The temperature parameter α has to be randomized $\alpha \sim p_\alpha$ so that a new neural distance can handle the joint distribution of Q^α and α . Accordingly, we have the family of joint densities $p_{Q^\alpha, \alpha}$ denoted by $\mathcal{P}_{Q^\alpha, \alpha}$. For sufficient flexibility of G , a mixture reference noise $Z_i^\alpha = \alpha Z_{i_1} + (1 - \alpha)Z_{i_2}$ is used where Z_{i_1} and Z_{i_2} are randomly drawn from p_Z . Then a neural distance specifically for parallel tempering is formulated as $d_{\mathcal{D}}(p_{Q^\alpha, \alpha}, p_{G(Z^\alpha, \alpha), \alpha}) = \sup_{D \in \mathcal{D}} \mathbf{E}_{Q^\alpha, \alpha}[D(Q^\alpha, \alpha)] - \mathbf{E}_{Z^\alpha, \alpha}[D(G(Z^\alpha, \alpha), \alpha)]$. In this revised framework, W_1 and V_1 adopt one more input dimension for receiving α . Our parallel training aims to solve

$$\min_{G \in \mathcal{G}} d_{\mathcal{D}}(p_{Q^\alpha, \alpha}, p_{G(Z^\alpha, \alpha), \alpha}). \quad (6)$$

If $\alpha = 1$ or $\alpha = 0$, the new optimization (6) reduces to the original problem (1); the original \hat{L}_b can be regarded as $\hat{L}_b^1(D^{(t)}, G^{(t)}) = \sum_{i=1}^{n_b} D^{(t)}(X_i, 1)/n_b - \sum_{j=1}^{m_b} D^{(t)}(G^{(t)}(Z_j, 1), 1)/m_b$. The optimization of D^* and G^* for (6) is carried out via the gradient-based update (2) w.r.t. $\hat{L}_b^\alpha(D^{(t)}, G^{(t)}) = \sum_{i=1}^{n_b} D^{(t)}(Q_i^{\alpha_i}, \alpha_i)/n_b - \sum_{j=1}^{m_b} D^{(t)}(G^{(t)}(Z_j^{\alpha_j}, \alpha_j), \alpha_j)/m_b$ where $Q_i^{\alpha_i} = \alpha_i X_{i_1} + (1 - \alpha_i)X_{i_2}$ and $Z_j^{\alpha_j} = \alpha_j Z_{j_1} + (1 - \alpha_j)Z_{j_2}$ for randomly chosen $X_{i_1}, X_{i_2} \in \mathbf{X}_{1:n}$, Z_{j_1}, Z_{j_2} from p_Z , and α_i, α_j from p_α . This update scheme remarks that the successfully learned generator synthesizes \mathcal{P}_{Q^α} because $\mathbf{w}^{(t)}$ and $\mathbf{v}^{(t)}$ are shared across the distributions having different levels of smoothness/multimodality. The importance of a convex input in generative modeling is partly discussed in An et al. (2020), asserting that the generator must

be discontinuous on singularity sets in \mathcal{Z} if \mathcal{X} is not convex. Then the neural-net-based generator might be fundamentally incompatible due to the universal approximation property of neural networks.

The distributional symmetricity of Q^α imposes a constraint to D and G as to the use of α . Considering $\alpha X_1 + (1 - \alpha)X_2 \stackrel{d}{=} (1 - \alpha)X_1 + \alpha X_2$ holds for any $0 \leq \alpha \leq 1$, ensuring $D(Q^\alpha, \alpha) \stackrel{d}{=} D(Q^{1-\alpha}, 1 - \alpha)$ and $G(Z^\alpha, \alpha) \stackrel{d}{=} G(Z^{1-\alpha}, 1 - \alpha)$ is desirable. By devising a transformation function $t(x)$ symmetric at 0.5 and plugging it into $D(Q^\alpha, t(\alpha)) \stackrel{d}{=} D(Q^{1-\alpha}, t(1 - \alpha))$ and $G(Z^\alpha, t(\alpha)) \stackrel{d}{=} G(Z^{1-\alpha}, t(1 - \alpha))$, the constraint can be satisfied. In this work, $t(x) = -2|x - 0.5| + 1$ is adopted for simulation studies.

In the ideal case, the perfectly learned $G(Z^\alpha, \alpha)$ recovers the ground-truth marginal distributions p_{Q^α} for all levels of α . However, it might not be achievable in practice on account of the finite sample size, the limited computing resources, and so forth. For instance, if $\alpha \sim \text{Unif}(0, 1)$, the training objective may need far longer iterations to successfully learn Q^α at $\alpha = 1$ or $\alpha = 0$ because X lies in the boundary in \mathcal{Q} . For these reasons, we suggest using a mixture-type distribution for α defined as follows:

$$\alpha \sim r\delta_1(\cdot) + (1 - r)p_{\alpha^*}(\cdot), \quad (7)$$

where $r \in [0, 1]$ and $\alpha^* \sim \text{Unif}(0, 1)$. Such specification of p_α naturally encourages the training process to concentrate more on the marginal distribution at $\alpha = 1$. Note r conceptually corresponds to the ratio of data instances picked from p_X in minibatches.

4.2 Reduction of gradients' variance

This section shows that our parallel tempering framework can enjoy improved training stability via reducing gradients' variance. Our analysis focuses on comparing gradients of $D^{(t)}$ when it comes with $\hat{L}_b^\alpha(D^{(t)}, G^{(t)})$ or $\hat{L}_b^1(D^{(t)}, G^{(t)})$, i.e., parallel tempering training

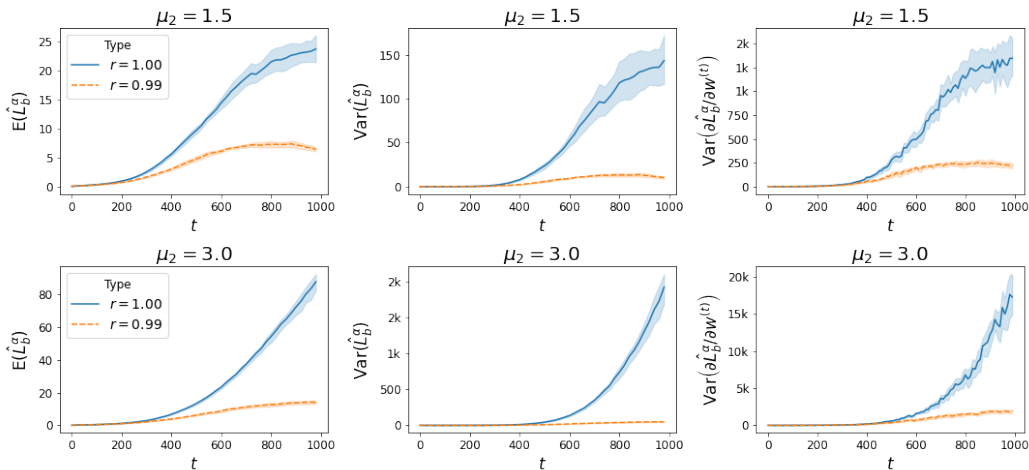


Figure 4: Comparison of $\hat{L}_b^\alpha(D^{(t)}, G^{(t)})$ and $\hat{L}_b^1(D^{(t)}, G^{(t)})$ on the toy example in Figure 2 with the same structure of \mathcal{D} : in the case of $r = 1$, minibatches consist of original samples. For the case of $r = 0.99$, there is only 1% of interpolated samples in each minibatch.

versus vanilla training. For fair and explicit comparison, we examine the behavior of one-step update $\mathbf{w}^{(t+1)}$ for \hat{L}_b^α and \hat{L}_b^1 respectively, updated from the exactly same configuration of $\mathbf{w}^{(t)}$. To be specific, we compare $\mathbf{w}^{(t+1)}|_{p_\alpha} = \mathbf{w}^{(t)} + \gamma_D \partial \hat{L}_b^\alpha(D^{(t)}, G^{(t)}) / \partial \mathbf{w}^{(t)}$ and $\mathbf{w}^{(t+1)}|_{\delta_1} = \mathbf{w}^{(t)} + \gamma_D \partial \hat{L}_b^1(D^{(t)}, G^{(t)}) / \partial \mathbf{w}^{(t)}$. The use of Q^α basically introduces some “bias” $\mathbf{E}(\mathbf{w}^{(t+1)}|_{p_\alpha}) - \mathbf{E}(\mathbf{w}^{(t+1)}|_{\delta_1})$ in the sense that the ultimate goal is to train a generative model under $\alpha = 1$ (i.e., $\mathbf{E}(\mathbf{w}^{(t+1)}|_{\delta_1})$ is the “gold standard” gradient). The bias disappears when $r = 1$ but would exist when $0 \leq r < 1$. The presence of the bias could be negative to learning the target marginal distribution $p_{X,1}$ because the tempering approach is essentially designed to learn the joint density of $p_{Q^{\alpha},\alpha}$ for the random α . But on the bright side, we find that the gradients’ variance can substantially decrease in general when $0 \leq r < 1$ as the below corollary substantiates. In this regard, the parameter r takes a central role in adjusting the *bias and variance trade-off* to learn $D(\cdot, 1)$ for the original data X .

Corollary 1. Under (A1-3), the size of gradients is bounded above by

$$\left| \frac{\partial \hat{L}_b^\alpha(D^{(t)}, G^{(t)})}{\partial W_{k,i,j}^{(t)}} \right| \leq C_{w,\kappa}(k) d_{\mathcal{D}}(p_{Q^{\alpha},\alpha}, p_{G^{(t)}(Z^{\alpha},\alpha)}) + O_p\left(\frac{1}{\sqrt{n_b}}\right), \quad (8)$$

for $k = 1, \dots, d$. Also, if $d_{\mathcal{D}}(p_{Q^{\alpha^*},\alpha^*}, p_{G^{(t)}(Z^{\alpha^*},\alpha^*)}) \leq d_{\mathcal{D}}(p_{X,1}, p_{G^{(t)}(Z,1),1})$ with (7), then $\hat{L}_b^\alpha(D^{(t)}, G^{(t)})$ has a smaller upper bound of the gradients' variance than $\hat{L}_b^1(D^{(t)}, G^{(t)})$.

Corollary 1 highlights that the variance can decrease particularly when the neural distance at $\alpha = 1$ is larger than the joint distance defined on $\alpha \sim p_{\alpha^*}$. The early training course and mode collapse are commonly under this condition. Figure 4 compares the expectation and the (gradients') variance of $\hat{L}_b^\alpha(D^{(t)}, G^{(t)})$ and $\hat{L}_b^1(D^{(t)}, G^{(t)})$ on the toy example introduced in Figure 2. In Figure 4, we see that the estimates of $d_{\mathcal{D}}$, i.e., $\mathbf{E}(\hat{L}_b^\alpha)$, become substantially smaller with $r = 0.99$ and in more severe multimodality as well, validating the variance reduction of the gradients suggested by Corollary 1. Moreover, the (gradients') variance of \hat{L}_b^α and \hat{L}_b^1 closely resemble the behavior of $\mathbf{E}(\hat{L}_b^\alpha)$ and $\mathbf{E}(\hat{L}_b^1)$, which also supports Corollary 1 that compares the size of gradients' variance by the upper bound.

The use of Q^α , however, does not always bring the variance reduction effects. There might be the reverse relationship $d_{\mathcal{D}}(p_{Q^{\alpha^*},\alpha^*}, p_{G^{(t)}(Z^{\alpha^*},\alpha^*)}) > d_{\mathcal{D}}(p_{X,1}, p_{G^{(t)}(Z,1),1})$, i.e., $G^{(t)}(Z, 1)$ is closer to X than $G^{(t)}(Z^\alpha, \alpha)$ to Q^α for $\alpha < 1$. For instance, if $G^{(t)}$ successfully covers \mathcal{S} , the condition may not hold. In this case, actually, the training does not obstinately need the variance reduction because the neural distance $d_{\mathcal{D}}(p_{X,1}, p_{G^{(t)}(Z,1),1})$ is sufficiently minimized yielding the small variance according to Corollary 1. More specific analysis within a linear class of D appears in Supplementary A.1, which shows a consistent conclusion.

The importance of variance reduction for gradients has been addressed mostly in the gradient-based optimization literature. In Yang et al. (2020), a class of nonconvex-nonconcave min-max optimization problems with the stochastic version of (2) is shown to have $O(\sigma_{\text{grad}}^2/t)$ convergence rate under the two-sided Polyak-Łojasiewicz condition w.r.t.

the loss function where σ_{grad}^2 upper bounds gradients' variance. For more details, refer to Yang et al. (2020) and reference therein.

4.3 Coherent training via regularization

Despite such statistical benefits of training with $p_{Q^\alpha, \alpha}$, the optimization (6) may fall into separate GAN training (w.r.t. each α). In other words, the optimization problem (6) reduces to learning $Q^\alpha | \alpha$ individually for every slice of α . In this case, there might be no guarantee that the use of interpolated variables contributes to the GAN training for p_X . For instance, for some specific α_1 and α_2 , imagine that the training at α_1 is complete but yet for $\alpha_2 \neq \alpha_1$. Then the equilibrium at α_1 might be compromised to promote the convergence at α_2 because the networks' parameters are shared for all α .

To prevent such a separate training system, we devise a novel penalty to maximize the potential of the parallel training (6). In a nutshell, an additional condition to D is imposed such that the learning process across different temperatures is at a similar pace. Given two samples X_1 and X_2 drawn from two distribution modes of target distributions, thus $\alpha X_1 + (1 - \alpha)X_2$ represents a sample from one distribution mode of p_{Q^α} for any α . The idea is to synchronize the learning pace across different α . As $D(\alpha X_1 + (1 - \alpha)X_2, \alpha)$ relates to how good the generator $G(\cdot, \alpha)$ learns the distribution mode represented by $\alpha X_1 + (1 - \alpha)X_2$, we regularize the coherency of D values for all α 's. That is, for $Q^{\alpha_1} = \alpha_1 X_1 + (1 - \alpha_1)X_2$ and $Q^{\alpha_2} = \alpha_2 X_1 + (1 - \alpha_2)X_2$ under the same (X_1, X_2) , we hope that $D(Q^{\alpha_1}, \alpha_1) \approx D(Q^{\alpha_2}, \alpha_2)$. Inspired by mean value theorem, we brutally approximate the difference between $D(Q^{\alpha_1}, \alpha_1)$ and $D(Q^{\alpha_2}, \alpha_2)$ by $\nabla_{Q^{\tilde{\alpha}}} D(Q^{\tilde{\alpha}}, \tilde{\alpha}) \cdot (Q^{\alpha_1} - Q^{\alpha_2})$ where $\tilde{\alpha} = \nu \alpha_1 + (1 - \nu) \alpha_2$ for some $\nu \in [0, 1]$, and thus place the following novel penalty when updating D ,

$$H = \lambda \mathbf{E}_{\alpha_1, \alpha_2, \nu} \mathbf{E}_{Q^{\tilde{\alpha}}} \left[\left(\nabla_{Q^{\tilde{\alpha}}} D(Q^{\tilde{\alpha}}, \tilde{\alpha}) \cdot (Q^{\alpha_1} - Q^{\alpha_2}) \right)^2 \right], \quad (9)$$

where $\alpha_1 \sim p_\alpha$, $\alpha_2 \sim \text{Unif}(0, 1)$, $\nu \sim \text{Unif}(0, 1)$, and λ is a hyperparameter to determine the impact of the penalty during the training. The detailed implementation with this suggested penalty appears in Algorithm 1 in Supplementary C. If $r = 1$, (9) reduces to the penalty suggested by Mescheder et al. (2018). We recommend $\lambda = 100$ as a default.

Remark 1. Note that $\nabla_{Q^{\tilde{\alpha}}} D(Q^{\tilde{\alpha}}, \tilde{\alpha}) \cdot (Q^{\alpha_1} - Q^{\alpha_2})$ can be rewritten as $(\alpha_1 - \alpha_2) \nabla_{Q^{\tilde{\alpha}}} D(Q^{\tilde{\alpha}}, \tilde{\alpha}) \cdot (X_1 - X_2)$. Thus, if X_1 and X_2 are far away from each other, i.e., two distanced distribution modes of p_X , the penalty is larger. Intuitively, the proposed coherency penalty is a weighted penalty w.r.t. between-mode distance, so it accommodates the multimodality of p_X .

Additionally, the penalty helps avoid compromising the convergence of other temperatures. Suppose that $\nabla_{Q^{\tilde{\alpha}}} D(Q^{\tilde{\alpha}}, \tilde{\alpha})$ and $(Q^{\alpha_1} - Q^{\alpha_2})$ are bounded. Then it follows that (9) $\rightarrow 0$ if and only if $\mathbf{E}_{\alpha_1, \alpha_2} \mathbf{E}_{Q^{\tilde{\alpha}}} [|\nabla_{Q^{\tilde{\alpha}}} D(Q^{\tilde{\alpha}}, \tilde{\alpha})|^2] \rightarrow 0$ for all ν by the (reversed) Cauchy-Schwarz inequality. This essentially implies that $\mathbf{E}_{Q^\alpha} [|\nabla_{Q^\alpha} D(Q^\alpha, \alpha)|^2]$ diminishes for all α simultaneously, so the training at least locally converges to the equilibrium for all α by Mescheder et al. (2018). Intuitively, in such a case, there would be no power to destroy the equilibria across all α . The penalty also naturally helps control the size of $M_w(l)$, so it further contributes to stabilizing the GAN training as discussed in Section 2.3.2.

4.4 Statistical analysis

In this section, we analyze the proposed distance in (6) and its estimation error within the size-independent sample complexity framework (Golowich et al., 2018; Ji et al., 2021). We show that the estimated generator with the neural distance (6) for parallel training achieves nearly min-max optimal. The employed theoretical framework readily adapts deep and wide neural networks by characterizing the sample complexity via the norm of weight matrices. In contrast to the prior works (Zhou et al., 2021; Metzger, 2022), our developed theory

does not necessitate impractical conditions. For example, the sample size must increase faster than or equal to the number of parameters. We remark that a lot of deployed neural networks in the real world nowadays have much more parameters than training samples.

To begin with, the set of i.i.d. samples of Q^α are constructed from $\mathbf{X}_{1:n}$. Without loss of generality, the sample size n is assumed even, so there is $n_e = n/2$ number of i.i.d. Q^α samples constructed by $Q_i^{\alpha_i} = \alpha_i X_{2i-1} + (1 - \alpha_i) X_{2i}$ for all $i = 1, \dots, n_e$. Let's denote by $d_{\mathcal{D}}(\hat{p}_{Q^\alpha, \alpha}, \hat{p}_{G(Z^\alpha, \alpha)}) = \sup_{D \in \mathcal{D}} \sum_{i=1}^{n_e} D(Q_i^{\alpha_i}, \alpha_i) n_e - \sum_{j=1}^m D(G(Z_j^{\alpha_j}, \alpha_j), \alpha_j) / m$ the empirical neural distance where \hat{p} implies the empirical mass function, and the estimator \hat{G}^* is determined by minimizing $d_{\mathcal{D}}(\hat{p}_{Q^\alpha, \alpha}, \hat{p}_{G(Z^\alpha, \alpha)})$. Note that the sample complexity analysis does not consider the minibatch scheme. The estimation error of \hat{G}^* can be characterized by the population-level neural distance. By referring to the work of Ji et al. (2021), we specifically write the estimation error as $d_{\mathcal{D}}(p_{Q^\alpha, \alpha}, p_{\hat{G}^*(Z^\alpha, \alpha), \alpha}) - \inf_{G \in \mathcal{G}} d_{\mathcal{D}}(p_{Q^\alpha, \alpha}, p_{G(Z^\alpha, \alpha), \alpha})$. For the simplicity of analysis, the proposed penalty term (9) is not considered. Let's further assume that

(A4) the activation functions κ_i and ψ_j are positive homogeneous for all i and j , i.e.,

$$\kappa_i(cx) = c\kappa_i(x) \text{ and } \psi_j(cx) = c\psi_j(x) \text{ for any } c \geq 0 \text{ and } x \in \mathbb{R}.$$

Relu and lRelu are representative examples satisfying this positive-homogeneous condition.

First, we find that the estimation error is bounded by the properties of \mathcal{D} and the sample size in a probability sense. Let's denote by $\mathcal{P}_{\mathcal{G}, \alpha}$ the family of densities $p_{G(Z^\alpha, \alpha), \alpha}$ for $G \in \mathcal{G}$.

Theorem 2. Under (A1-4), let \mathcal{G} be sufficiently large such that $p_{Q^\alpha, \alpha} \in \mathcal{P}_{\mathcal{G}, \alpha}$ and the number m of samples drawn from the distribution p_z scales faster than n_e . Then

$$d(p_{Q^\alpha, \alpha}, p_{\hat{G}^*(Z^\alpha, \alpha), \alpha}) = O_p \left(\frac{\prod_{l=1}^d M_w(l) \prod_{s=1}^{d-1} K_\kappa(s) \sqrt{B_X^2 + 1} (2\sqrt{3d} + \sqrt{\log(1/\delta)})}{\sqrt{n_e}} \right), \quad (10)$$

with the probability $1 - 2\delta$.

Interestingly, the estimation error may not increase much although the critic uses a deeper network since the error depends on \sqrt{d} . The assumption that m scales faster than n_e is mild. With sufficient computing resources, it is easy to set the sufficiently large number of iterations T such that $m = n_b \times T \gg n_e$.

Lastly, we present the minimax lower bound in the following Theorem 3. Suppose that $\mathcal{P}_{Q^\alpha, \alpha}$ is the family of Borel probability measures over the domain $\mathcal{Q} \times [0, 1]$.

Theorem 3. Under (A1-4), let \hat{p}_{n_e} be any estimator of the target distribution $p_{Q^\alpha, \alpha}$ constructed based on the n_e size of random samples. Then,

$$\inf_{\hat{p}_{n_e}} \sup_{p_{Q^\alpha, \alpha} \in \mathcal{P}_{Q^\alpha, \alpha}} P \left[d_{\mathcal{D}}(p_{Q^\alpha, \alpha}, \hat{p}_{n_e}) \geq \frac{C_{\text{LB}}}{\sqrt{n_e}} \right] > 0.55, \quad (11)$$

where $C_{\text{LB}} = \log 2 |c(C_X^2) + c(B_X^2) + c(1 - B_X^2) + c(-B_X^2)| / 160$ with $C_X = \sqrt{B_X^2 + 1}$ and $c(x) = M_w(d)(\kappa_{d-1}(\cdots \kappa_1(M_w(1)x/C_X)))$.

The proof is based on applying Fano's lemma with a hypothetical joint density of Q^α and α . In conjunction with Theorem 2, we observe that the estimated generator achieves the nearly optimal $\sqrt{n_e}$ -minimax rate. For a Relu-based critic, the bounds in (10) and (11) explicitly share the term $\prod_{l=1}^d M_w(l)$ and $\sqrt{n_e}$. Our minimax analysis matches the results found in Ji et al. (2021), which advertises that the parallel framework with (6) preserves the same minimax rate of convergence.

5 Simulation Studies

Simulation setups, such as network architectures, evaluation metrics (e.g., IS, FID, Pareto frontier), competing models, etc. are detailed further in Supplementary D.

5.1 Data generation

Image Data Generation Our first study works on image data generation with the popular benchmark datasets: **CIFAR10** and **TinyImageNet**. Each comprises 60k $32 \times 32 \times 3$ images across 10 classes and 100k $64 \times 64 \times 3$ across 200 classes respectively. Intuitively, the different classes shape multimodal p_X . The standard computer vision metrics, Inception Score (IS) and Fréchet Inception Distance (FID), are measured. Higher IS and smaller FID indicate superior performance. The following popular GAN metrics, the Jensen-Shannon divergence (JSD) and the Pearson χ^2 -divergence (PD, Mao et al., 2017), are also considered to show the general applicability of PTGAN. Note ND abbreviates the neural distance.

PTGAN is compared to generally applicable decent competitors. The spectral normalization (SN, Miyato et al., 2018) frequently used in the state-of-the-art models, e.g., StyleGAN-XL (Sauer et al., 2022), is contrasted. As the strongest penalty-based GAN framework to our knowledge, the Lipschitz GAN (Zhou et al., 2019), imposing a maximum penalty (MP) of D 's gradient norm, is chosen as a competitor. Also, the technique of adding a learnable noise ϵ to X (LN, Jenni and Favaro, 2019), i.e., training with $p_{X+\epsilon}$, is considered. For fair comparison, the CNN-based structures of D and G used in Miyato et al. (2018) are employed by all approaches. PT and CP represent the proposed objective (6) and the coherency penalty (9) respectively. To investigate CP's effects, we test PT with MP and the common gradient penalty (GP, Gulrajani et al., 2017) only suitable for ND. For PT, $r = 0.99$ is set, so the interpolated data points comprise 1% of each minibatch.

Remarkably, PTGAN (PT+CP) outperforms the competitors in all combinations of benchmark datasets and GAN metrics (Table 1). In particular, PTGAN achieves notable IS/FID scores when coupled with CP. Figure 5 supports these results by showing a significant decrease in variance with $r = 0.99$. Table 6 in Supplementary D.2.1 further compares the

training with $r = 0.9$ or $r = 1$, showing $r = 1$ yields similar performance with MP.

Table 1: Summary of IS/FID: the best scores are averaged across 10 independent runs, and standard deviations are in the parentheses.

		CIFAR10		TinyImageNet	
$d_{\mathcal{D}}$	Type	IS (\uparrow)	FID (\downarrow)	IS (\uparrow)	FID (\downarrow)
JSD	SN	6.513 (0.350)	34.205 (4.563)	4.866 (0.307)	150.208 (5.423)
	LN	5.562 (0.213)	60.949 (7.239)	4.671 (0.175)	151.474 (5.662)
	MP	6.768 (0.081)	30.209 (0.550)	7.138 (0.139)	107.857 (1.352)
	PT + MP	6.727 (0.067)	30.314 (0.663)	7.263 (0.193)	105.723 (1.894)
	PT + CP	7.349 (0.110)	24.060 (0.815)	7.741 (0.182)	99.838 (1.092)
PD	SN	6.611 (0.336)	33.959 (5.361)	2.835 (1.795)	304.985 (153.515)
	LN	5.032 (1.983)	134.073 (173.329)	3.212 (2.192)	312.9 (174.352)
	MP	6.850 (0.117)	29.563 (0.589)	7.141 (0.120)	106.093 (1.764)
	PT + MP	6.779 (0.082)	29.932 (0.669)	7.204 (0.145)	105.776 (1.128)
	PT + CP	7.429 (0.084)	23.280 (0.883)	7.563 (0.150)	101.013 (1.42)
ND	SN	5.591 (0.198)	45.868 (2.148)	4.348 (0.244)	177.594 (8.918)
	LN	4.513 (0.317)	80.094 (5.243)	4.047 (0.362)	181.511 (14.373)
	MP	6.929 (0.123)	28.777 (1.010)	7.339 (0.171)	103.936 (1.198)
	GP	6.797 (0.106)	29.814 (0.933)	7.274 (0.122)	104.896 (1.409)
	PT + MP	6.923 (0.089)	28.422 (0.961)	7.398 (0.172)	103.720 (1.711)
	PT + GP	6.767 (0.096)	29.731 (0.661)	7.092 (0.122)	106.529 (1.855)
	PT + CP	7.292 (0.090)	24.838 (0.866)	7.668 (0.119)	100.364 (2.453)

Tabular Data Generation PTGAN’s performance is assessed in generating tabular data for supervised learning, on three benchmark datasets: **Adult** for income prediction, **Credit Card Default** for default prediction, and **Law School Admission** for admission

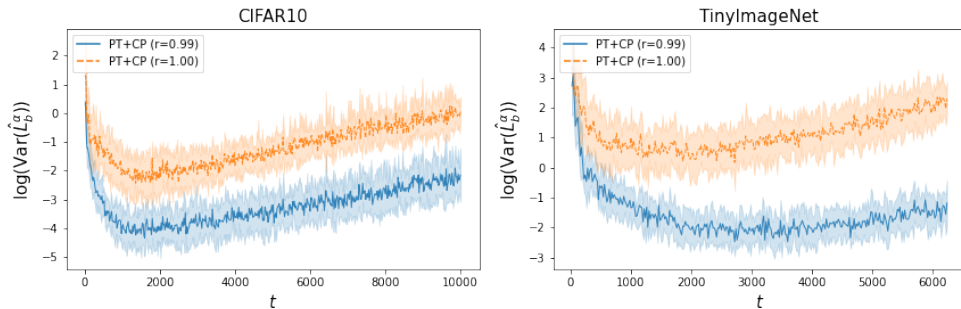


Figure 5: Variance reduction: the logarithm of $\text{Var}(\hat{L}_b^\alpha)$ over training iterations. Shaded areas indicate one standard deviation from the straight average lines.

prediction. Each dataset is split 90%/10% for training D_{train} and test data D_{test} respectively. GAN models with fully connected layers for both D and G are trained on D_{train} with ND. For PTGAN, r is set to 0.5. We denote by D_t the output of $G^{(t)}$ with 1k instances. For downstream evaluation at the t th iteration, random forest (RF), support vector machine (SVM), and logistic regression (LR) are trained on both D_{train} and D_t . Then the area under the ROC curve (AUC) for these models is measured on D_{test} . These AUC scores are denoted as S_{train} and S_t respectively. We calculate $S_T = \sum_{t=\lceil T/2 \rceil+1}^T |S_{\text{train}} - S_t| / (T - \lceil T/2 \rceil + 2)$ that implicitly evaluates the quick and accurate convergence of GAN models for the downstream task. Only MP is considered for comparison because of its superiority over other competitors in the previous section. Table 2 summarizes S_T from 10 independent runs, indicating PTGAN consistently outperforms MP across all datasets and predictive models. In Supplementary D.2.2, Table 8 demonstrates PTGAN’s superiority for JSD or PD as well, and Table 9 summarizes S_T of MP with different penalty parameters but still defeated by PTGAN.

Table 2: Summary of \mathbf{S}_T : all scores are averaged across 10 replicated implementations, and standard deviations appear in the parentheses. Smaller scores are preferred.

Data	Type	RF (\downarrow)	SVM (\downarrow)	LR (\downarrow)
Adult	PT + CP	0.022 (0.004)	0.038 (0.007)	0.028 (0.002)
	MP	0.047 (0.029)	0.060 (0.025)	0.050 (0.029)
Law School	PT + CP	0.018 (0.007)	0.024 (0.007)	0.006 (0.002)
	MP	0.096 (0.018)	0.099 (0.024)	0.069 (0.023)
Credit Card	PT + CP	0.062 (0.008)	0.071 (0.018)	0.038 (0.010)
	MP	0.159 (0.040)	0.168 (0.047)	0.147 (0.043)

5.2 Fair data generation

The intriguing property of PTGAN, learning $\mathcal{P}_{Q^\alpha, \alpha}$, can open up new generative modeling tasks. This work primarily focuses on fair data generation that has recently seen a growing demand for morality control in machine learning models. In algorithmic fairness, a key focus aims to minimize discrimination by decision models, denoted as h , against minor groups. We pay attention to a classification problem; $C \in \mathcal{C}$ represents covariates, $A \in \{0, 1\}$ is a binary sensitive attribute (e.g., race or gender), $Y \in \{0, 1\}$ is a binary outcome, and $h : \mathcal{C} \rightarrow [0, 1]$ is learned to predict Y . The goal is to ensure statistical independence between $h(C)$ and A , so h returns fair outcomes regardless of A . Discrimination is measured by $|\mathbf{E}(\hat{Y}|A = 1) - \mathbf{E}(\hat{Y}|A = 0)|$ where $\hat{Y} = 1(h(C) > \tau)$ for some τ . This measurement, called statistical/demographic parity (SP), tends to compromise the model’s utility, such as classification accuracy. For more details and recent studies on algorithmic fairness, see Barocas et al. (2017); Sohn et al. (2023) and reference therein.

Interestingly, the PTGAN framework can be used to enable G to produce various levels of fair synthetic data while holding the training stability. Let’s denote by $X_i^{(j)} = (C_i^{(j)}, j, Y_i^{(j)})$

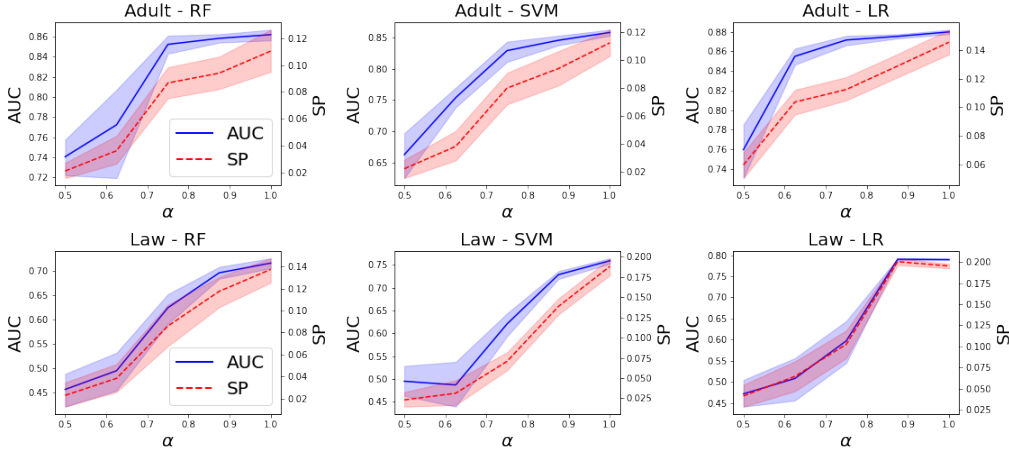


Figure 6: The trade-off curves between AUC and SP for the downstream classifiers.

the tuple of the j th group for $j = 0, 1$, and define $\check{X}_i^\alpha = \alpha X_i^{(0)} + (1 - \alpha)X_j^{(1)}$ and $\check{X}_i^{1-\alpha} = (1 - \alpha)X_i^{(0)} + \alpha X_j^{(1)}$. By creating Q^α as an equal mixture of \check{X}_i^α and $\check{X}_i^{1-\alpha}$, PTGAN can synthesize fair data sets with α measuring the level of fairness. To clarify the underlying fairness mechanism, let's consider the exemplary situations with the data points $(c_0, 0, y_0)$ and $(c_1, 1, y_1)$: (i) $c_0 = c_1, y_0 = y_1$, (ii) $c_0 \neq c_1, y_0 = y_1$, (iii) $c_0 = c_1, y_0 \neq y_1$, and (iv) $c_0 \neq c_1, y_0 \neq y_1$. Case (iii) explicitly contributes to discrimination, as A directly determines Y ; (i) avoids discrimination. (ii) and (iv) permit dependency between C and A , allowing discrimination through C . In this regard, Q^α removes such dependency observed in (ii), (iii), and (iv) for $0 < \alpha < 1$ while preserving the relationship between Y and C in (i).

Our FairPTGAN framework is verified by comparing the behavior of trade-offs between utility and fairness to a recent fair generative model (FairWGANGP, Rajabi and Garibay, 2022) and a seminar preprocessing method (GeoRepair, Feldman et al., 2015). FairWGANGP places a penalty term $\lambda_f |\mathbf{E}(\tilde{Y}|\tilde{A} = 1) - \mathbf{E}(\tilde{Y}|\tilde{A} = 0)|$ when updating $G^{(t)}$ where $(\tilde{C}, \tilde{A}, \tilde{Y}) \sim G^{(t)}(Z)$, so that $G^{(t)}$ produces societally unbiased synthetic data. GeoRepair solves a Wasserstein-median problem between $C|A = 1$ and $C|A = 0$ with a weighting parameter $\lambda_p \in [0, 1]$. For PTGAN, $r = 0.2$ is set to encourage the generator to learn the

intermediate (fair) distributions more effectively. For evaluation, the Pareto frontiers of AUC and SP are adopted as in Sohn et al. (2023), where the cutting-off parameter τ is chosen to maximize AUC. All methods have 10 independent runs. In each run, 90% of data is used to train generative models whose last iterate produces 1k synthetic entities to train downstream models. Then the Pareto frontiers are found by evaluating AUC and SP of the downstream models on the remaining 10% test data. GeoRepair is applied to the FairPTGAN model with $\alpha = 1$.

FairPTGAN proves computationally efficient and achieves favorable Pareto frontiers. Table 3 indicates that ours have smaller statistical parity (SP) values than competitors for certain utility thresholds. We remark that the joint learning structure in (6) allows FairPTGAN’s generator to produce synthetic datasets with different fairness levels just by varying α of $G^{(t)}(Z^\alpha, \alpha)$ (i.e., achieving a different balance for the fairness-utility trade-off). In contrast, FairWGANGP requires retraining when λ_f changes. GeoRepair also has to repeat the processing whenever λ_p changes as well. Although GeoRepair may take some advantages of being model-free, its computational cost gets brutally expensive as the number of entities and variables in data increases. Additionally, GeoRepair ignores the multivariate structure of C , which may lead to sacrificing too much utility.

6 Conclusion

In this work, we demystify how mode collapse stirs the inflation of the gradients’ variance of the critic function by investigating the impact of the remaining neural distance toward missing support. As an explicit remedy that shortens the remaining distance, PTGAN builds the bridge connecting all modes in p_X via the convex interpolation. We theoretically justify that the proposed framework enjoys the variance reduction effects of gradients.

Table 3: Averages of the 10 smallest SP scores whose AUCs are greater than the thresholds (≥ 0.85 for Adult and ≥ 0.65 for Law School). Standard deviations are in the parentheses. Table 10 in Supplementary D.3 presents consistent results with different thresholds.

Data	Model	RF (\downarrow)	SVM (\downarrow)	LR (\downarrow)
Adult	FairPTGAN	0.064 (0.006)	0.077 (0.014)	0.084 (0.006)
	FairWGANGP	0.083 (0.010)	0.088 (0.010)	0.095 (0.005)
	GeoRepair	0.082 (0.012)	0.089 (0.009)	0.106 (0.009)
Law School.	FairPTGAN	0.054 (0.014)	0.056 (0.006)	0.079 (0.020)
	FairWGANGP	0.105 (0.006)	0.115 (0.007)	0.175 (0.003)
	GeoRepair	0.102 (0.011)	0.129 (0.013)	0.187 (0.003)

Rather than struggling to achieve the state-of-the-art scores of IS/FID or AUC on various challenging data sets, our work concentrates on clarifying the training improvement by leveraging tempered target distributions with the minimal use of extra training tricks. Finally, we introduce the fair data generation task as an intriguing variant of PTGAN that addresses the importance and necessity of the generator’s capability to produce intermediate distributions beyond enhancing training stability.

References

- An, D., Guo, Y., Lei, N., Luo, Z., Yau, S., and Gu, X. (2020). Ae-ot: a new generative model based on extended semi-discrete optimal transport. In *Proceedings of the 8th International Conference on Learning Representations*. OpenReview.net.
- Arjovsky, M. and Bottou, L. (2017). Towards principled methods for training generative

- adversarial networks. In *Proceedings of the 5th International Conference on Learning Representations*. OpenReview.net.
- Arjovsky, M., Chintala, S., and Bottou, L. (2017). Wasserstein generative adversarial networks. In *Proceedings of the 34th International Conference on Machine Learning*, volume 70 of *Proceedings of Machine Learning Research*, pages 214–223. PMLR.
- Arora, S., Ge, R., Liang, Y., Ma, T., and Zhang, Y. (2017). Generalization and equilibrium in generative adversarial nets (gans). In *Proceedings of the 34th International Conference on Machine Learning*, volume 70 of *Proceedings of Machine Learning Research*, pages 224–232. PMLR.
- Ashman, K. A., Bird, C. M., and Zepf, S. E. (1994). Detecting bimodality in astronomical datasets. *The Astronomical journal*, 108(6):2348–.
- Barocas, S., Hardt, M., and Narayanan, A. (2017). Fairness in machine learning. *Nips tutorial*, 1:2017.
- de Rosa, G. H. and Papa, J. P. (2021). A survey on text generation using generative adversarial networks. *Pattern Recognition*, 119:108098.
- Deng, W., Zhang, Q., Feng, Q., Liang, F., and Lin, G. (2023). Non-reversible parallel tempering for deep posterior approximation. In *Proceedings of the AAAI Conference on Artificial Intelligence*, pages 7332–7339. AAAI Press.
- Feldman, M., Friedler, S. A., Moeller, J., Scheidegger, C., and Venkatasubramanian, S. (2015). Certifying and removing disparate impact. In *Proceedings of the 21th ACM SIGKDD International Conference on Knowledge Discovery and Data Mining*, pages 259–268. ACM.

- Geyer, C. J. (1991). Markov chain monte carlo maximum likelihood.
- Golowich, N., Rakhlin, A., and Shamir, O. (2018). Size-independent sample complexity of neural networks. In *Conference On Learning Theory*, volume 75 of *Proceedings of Machine Learning Research*, pages 297–299. PMLR.
- Goodfellow, I., Pouget-Abadie, J., Mirza, M., Xu, B., Warde-Farley, D., Ozair, S., Courville, A., and Bengio, Y. (2014). Generative adversarial nets. In *Advances in Neural Information Processing Systems*, volume 27. Curran Associates, Inc.
- Goodfellow, I. J. (2017). NIPS 2016 tutorial: Generative adversarial networks. *CoRR*, abs/1701.00160.
- Gulrajani, I., Ahmed, F., Arjovsky, M., Dumoulin, V., and Courville, A. C. (2017). Improved training of wasserstein gans. In *Advances in Neural Information Processing Systems*, volume 30. Curran Associates, Inc.
- Hwang, D. Y., Nechaev, Y., de Lichy, C., and Zhang, R. (2023). Gan-lm: Generative adversarial network using language models for downstream applications. In *Proceedings of the 16th International Natural Language Generation Conference*, pages 69–79.
- Jabbar, A., Li, X., and Omar, B. (2021). A survey on generative adversarial networks: Variants, applications, and training. *ACM Computing Surveys (CSUR)*, 54(8):1–49.
- Jenni, S. and Favaro, P. (2019). On stabilizing generative adversarial training with noise. In *Proceedings of the IEEE/CVF Conference on Computer Vision and Pattern Recognition*, pages 12145–12153. Computer Vision Foundation / IEEE.
- Ji, K., Zhou, Y., and Liang, Y. (2021). Understanding estimation and generalization error of generative adversarial networks. *IEEE Trans. Inf. Theory*, 67(5):3114–3129.

- Jordon, J., Szpruch, L., Houssiau, F., Bottarelli, M., Cherubin, G., Maple, C., Cohen, S. N., and Weller, A. (2022). Synthetic data – what, why and how?
- Kang, M., Zhu, J., Zhang, R., Park, J., Shechtman, E., Paris, S., and Park, T. (2023). Scaling up gans for text-to-image synthesis. In *Proceedings of the IEEE/CVF Conference on Computer Vision and Pattern Recognition*, pages 10124–10134. IEEE.
- Kim, S., Song, Q., and Liang, F. (2023). A new paradigm for generative adversarial networks based on randomized decision rules. *CoRR*, abs/2306.13641.
- Liang, F., Cheng, Y., and Lin, G. (2014). Simulated stochastic approximation annealing for global optimization with a square-root cooling schedule. *Journal of the American Statistical Association*, 109(506):847–863.
- Mao, X., Li, Q., Xie, H., Lau, R. Y. K., Wang, Z., and Smolley, S. P. (2017). Least squares generative adversarial networks. In *Proceedings of the IEEE international conference on computer vision*, pages 2813–2821. IEEE Computer Society.
- Mescheder, L. M., Geiger, A., and Nowozin, S. (2018). Which training methods for gans do actually converge? In *Proceedings of the 35th International Conference on Machine Learning*, volume 80 of *Proceedings of Machine Learning Research*, pages 3478–3487. PMLR.
- Metzger, J. (2022). Adversarial estimators. *arXiv preprint arXiv:2204.10495*.
- Miyato, T., Kataoka, T., Koyama, M., and Yoshida, Y. (2018). Spectral normalization for generative adversarial networks. In *Proceedings of the 6th International Conference on Learning Representations*. OpenReview.net.

- Mottini, A., Lheritier, A., and Acuna-Agost, R. (2018). Airline passenger name record generation using generative adversarial networks. *arXiv preprint arXiv:1807.06657*.
- Neal, R. M. (1996). Sampling from multimodal distributions using tempered transitions. *Statistics and computing*, 6:353–366.
- Nowozin, S., Cseke, B., and Tomioka, R. (2016). f-gan: Training generative neural samplers using variational divergence minimization. In *Advances in Neural Information Processing Systems 29*, pages 271–279.
- Rajabi, A. and Garibay, Ö. Ö. (2022). Tabfairgan: Fair tabular data generation with generative adversarial networks. *Mach. Learn. Knowl. Extr.*, 4(2):488–501.
- Roth, K., Lucchi, A., Nowozin, S., and Hofmann, T. (2017). Stabilizing training of generative adversarial networks through regularization. In *Advances in Neural Information Processing Systems 30*, pages 2018–2028.
- Sajjadi, M. S. M., Parascandolo, G., Mehrjou, A., and Schölkopf, B. (2018). Tempered adversarial networks. In *Proceedings of the 35th International Conference on Machine Learning*, volume 80 of *Proceedings of Machine Learning Research*, pages 4448–4456. PMLR.
- Sauer, A., Schwarz, K., and Geiger, A. (2022). Stylegan-xl: Scaling stylegan to large diverse datasets. In *ACM SIGGRAPH 2022 Conference Proceedings*, pages 1–10.
- Sohn, J., Song, Q., and Lin, G. (2023). Fair supervised learning with a simple random sampler of sensitive attributes. *arXiv preprint arXiv:2311.05866*.
- Wang, J., Wen, S., Symmans, W. F., Pusztai, L., and Coombes, K. R. (2009). The

- bimodality index: a criterion for discovering and ranking bimodal signatures from cancer gene expression profiling data. *Cancer informatics*, 7:CIN–S2846.
- Wang, Y. and Ročková, V. (2022). Adversarial bayesian simulation. *arXiv preprint arXiv:2208.12113*.
- Yang, J., Kiyavash, N., and He, N. (2020). Global convergence and variance reduction for a class of nonconvex-nonconcave minimax problems. In *Advances in Neural Information Processing Systems 33*.
- Zhang, H., Cissé, M., Dauphin, Y. N., and Lopez-Paz, D. (2018). mixup: Beyond empirical risk minimization. In *Proceedings of the 6th International Conference on Learning Representations*. OpenReview.net.
- Zhao, Y., Xie, J., and Li, P. (2023). Coopinit: Initializing generative adversarial networks via cooperative learning. In *Proceedings of the AAAI Conference on Artificial Intelligence*, volume 37, pages 11345–11353.
- Zhao, Z., Kumar, A., Birke, R., and Chen, L. Y. (2021). CTAB-GAN: effective table data synthesizing. In *Asian Conference on Machine Learning*, volume 157 of *Proceedings of Machine Learning Research*, pages 97–112. PMLR.
- Zhou, X., Jiao, Y., Liu, J., and Huang, J. (2021). A deep generative approach to conditional sampling. *Journal of the American Statistical Association*, 118:1837 – 1848.
- Zhou, Z., Liang, J., Song, Y., Yu, L., Wang, H., Zhang, W., Yu, Y., and Zhang, Z. (2019). Lipschitz generative adversarial nets. In *Proceedings of the 36th International Conference on Machine Learning*, volume 97 of *Proceedings of Machine Learning Research*, pages 7584–7593. PMLR.

SUPPLEMENTARY MATERIAL

Title: Parallely Tempered Generative Adversarial Networks

A Additional Discussion

A.1 Variance reduction within a linear class

As a more concrete example, we further investigate the variance reduction mechanism under the linear function class \mathcal{D} . Let's suppose $D(Q^\alpha, \alpha) = W_1^\top [Q^\alpha, \alpha]$ with $W_1 \in \mathbb{R}^{(d_X+1) \times 1}$ and also $G^{(t)}(\alpha Z_1 + (1 - \alpha)Z_2, \alpha) \stackrel{d}{=} \alpha G^{(t)}(Z_1, 1) + (1 - \alpha)G^{(t)}(Z_2, 1)$, which means $G^{(t)}$ is simultaneously converging to the equilibrium for all α . Then the below proposition shows when the gradients' variance reduction occurs under the verifiable assumption.

Proposition 3. Suppose D is linear, $n_b = m_b$, and $G^{(t)}(\alpha Z_1 + (1 - \alpha)Z_2, \alpha) \stackrel{d}{=} \alpha G^{(t)}(Z_1, 1) + (1 - \alpha)G^{(t)}(Z_2, 1)$. Then, $\text{tr} \left(\text{Cov} \left(\frac{\partial \hat{L}_b^\alpha(D^{(t)}, G^{(t)})}{\partial W_1} \right) \right)$ is equal to

$$\left(\frac{2}{3} + \frac{1}{3}r \right) \text{tr} \left(\text{Cov} \left(\frac{\partial \hat{L}_b^1(D^{(t)}, G^{(t)})}{\partial W_1} \right) \right) + \text{Var}(\alpha_1) \left(\frac{1}{n_b} + \frac{1}{m_b} \right).$$

This proposition shows that $\text{tr} \left(\text{Cov} \left(\frac{\partial \hat{L}_b^\alpha(D^{(t)}, G^{(t)})}{\partial W_1} \right) \right) \leq \text{tr} \left(\text{Cov} \left(\frac{\partial \hat{L}_b^1(D^{(t)}, G^{(t)})}{\partial W_1} \right) \right)$ holds for any r if $\text{tr}(\text{Cov}(X_1)) + \text{tr}(\text{Cov}(G^{(t)}(Z, 1))) > 2\text{Var}(\alpha_1)$ is satisfied, where the equality only holds with $r = 1$. The variance reduction effect tends to be stronger as $r \rightarrow 0$ and maximally decreases by $\frac{2}{3}$ factor. The extra assumption demands that the randomness of α does not have to dominate the randomness from X_1 and $G^{(t)}(Z, 1)$. This assumption is usually satisfied in deep learning applications; it is a convention to standardize the input space such that $\max(X) = 1$ and $\min(X) = -1$ (or $\min(X) = 0$ for efficient optimization. Also, the input dimension d_X is usually large, e.g., CIFAR10 (a benchmark data set in Section 5 with $d_X = 32 \times 32 \times 3$). By choosing $\text{Var}(\alpha) \leq \frac{1}{4}$, the assumption in the proposition is mild.

A.2 Comparison to Mixup

The idea of interpolating data points was first introduced by Zhang et al. (2018). They mainly discussed that the use of the convex combinations, so-called *Mixup*, greatly improves generalization errors and robustness against adversarial testing data within the supervised learning framework. Based on the idea of Mixup, there has been a strand of research designing better “mixed” data augmentation, mostly focusing on computer vision tasks (e.g., Yun et al., 2019; Verma et al., 2019; Hendrycks et al., 2020). It is worth mentioning that the original work of Zhang et al. (2018) also briefly discussed applying the Mixup technique for GAN training by introducing linear combinations of real and generated data points. Despite the similarity of Mixup and our convex mixture (5), there are fundamental differences: Mixup technique serves as a penalization that aims to regularize and smooth the optimization objective and hence to improve the generalization and robustness; in contrast, our usage of convex combination doesn’t change the optimization objective but creates auxiliary intermediate distributions that helps stabilize and accelerate the original GAN training. Refer to the below simulation for a direct simulation comparison between the Mixup and our approach.

Simulation setup & Result The toy data used to show Figure 1 is considered. Also, the network architectures of D and G in the figure are used. The Adam optimizer’s hyperparameters are set to $\beta_1 = 0.0$ and $\beta_2 = 0.9$ with the learning rates for D and G as 0.0001 (Kingma and Ba, 2015). Figure 7 illustrates the distributions G recovers over the different training iteration. The figure implies that the PTGAN scheme more quickly captures the entire distribution and begins to represent each unimodal component.

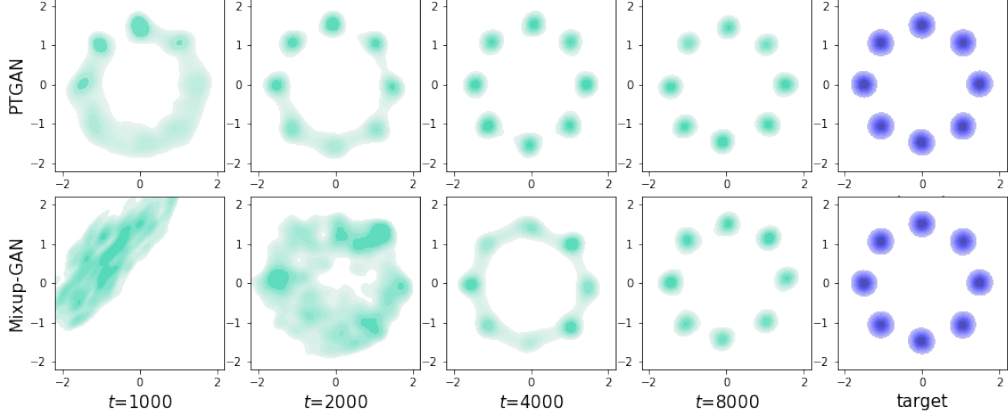


Figure 7: Plots drawn with lighter colors depict the kernel density plots of generated distributions by $G^{(t)}$ for the target distribution shown in the rightmost column.

B Proof

B.1 Proposition 1

For two distributions $X \sim p_1(x; \mu_1, \sigma_1^2)$ and $Y \sim p_2(x; \mu_2, \sigma_2^2)$ belonging to a location-scale invariant family, the second-order Wasserstein distance is equal to $\sqrt{(\mu_2 - \mu_1)^2 + (\sigma_2 - \sigma_1)^2}$ by Dowson and Landau (1982). Suppose (A1) and (A2). For any probability densities p_1 and p_2 ,

$$\begin{aligned}
 \mathbf{E}_{p_1}[D(X)] - \mathbf{E}_{p_2}[D(Y)] &\leq \int (D(x) - D(y))p_{12}(x, y)dxdy, \\
 &\leq \prod_{s=1}^d M_w(s) \prod_{u=1}^{d-1} K_\kappa(u) \int |x - y|p_{12}(x, y)dxdy, \\
 &= \prod_{s=1}^d M_w(s) \prod_{u=1}^{d-1} K_\kappa(u) \mathbf{E}|X - Y|,
 \end{aligned}$$

by the Cauchy-Schwarz inequality, and it implies

$$d_{\mathcal{D}}(p_1, p_2) \leq \prod_{s=1}^d M_w(s) \prod_{u=1}^{d-1} K_\kappa(u) \times W_1(p_1, p_2),$$

where $W_k(p_1, p_2)$ is the k th-order Wasserstein distance between p_1 and p_2 . Since $W_1(p_1, p_2) \leq W_p(p_1, p_2)$ for all $p \geq 1$, we obtain

$$d_{\mathcal{D}}(p_1, p_2) \leq \prod_{s=1}^d M_w(s) \prod_{u=1}^{d-1} K_{\kappa}(u) \sqrt{(\mu_1 - \mu_2)^2 + (\sigma_2 - \sigma_1)^2}.$$

Let's denote by \mathcal{L} the class of 1-Lipschitz continuous functions. It has been well-known that neural networks have the universal approximation property under the compact domain \mathcal{X}^1 (Lu et al., 2017; Park et al., 2021). Thus there is an approximation error $\delta_{\mathcal{D}}/2 > 0$ of \mathcal{D} to \mathcal{L} characterized by the structure of \mathcal{D} , i.e., for any function $f \in \mathcal{L}$, there always exists a network $D \in \mathcal{D}$, such that $|f(x) - D(x)| \leq \delta_{\mathcal{D}}/2$ for all $x \in \mathcal{X}$. Such an approximation holds due to the universal approximation properties of neural network (e.g., Park et al., 2021). Trivially, this implies that $|d_{\mathcal{D}}(p_1, p_2) - d_{\mathcal{L}}(p_1, p_2)| < \delta_{\mathcal{D}}$. Since $W_1(p_1, p_2) = d_{\mathcal{L}}(p_1, p_2)$, we obtain the bound, $W_1(p_1, p_2) - \delta_{\mathcal{D}} \leq d_{\mathcal{D}}(p_1, p_2)$. Moreover, since $W_1(p_1, p_2) \geq |\mu_1 - \mu_2|$ by Lemma II.2 in Chhachhi and Teng (2023), we obtain the result in the statement.

B.2 Proposition 2

The argument in the main text is based on the following two lemmas.

Lemma 1. Assume $\|w_d^{(t)}\| > 0$. The norm of the covariance of the w_d 's gradient is bounded below

$$\left\| \text{Cov} \left(\frac{\partial \hat{L}_b(D^{(t)}, G^{(t)})}{\partial w_d^{(t)}} \right) \right\|_2 \geq \frac{\text{Var}(\hat{L}_b(D^{(t)}, G^{(t)}))}{\|w_d^{(t)}\|^2},$$

where the $\|\cdot\|_2$ for the covariance matrix is the induced 2-norm.

¹It is assumed that the location-scale distributions have a compact support. In general, if the compact set is sufficiently large compared with the scale of the distribution, this assumption is practically reasonable. For instance, the 2- and 8- normal mixtures in Figure 3.

Proof. Let $\hat{L}_i = D(X_i) - D(G(Z_i))$ and $\hat{L}_{d-1,i} = D_{d-1}(X_i) - D_{d-1}(G(Z_i))$ where D_{d-1} is the output of the $(d-1)$ th hidden layer. Since $\partial \hat{L}_i / \partial w_d^\top = \hat{L}_{d-1,i}$ and $\hat{L}_i = w_d^\top \hat{L}_{d-1,i}$,

$$\begin{aligned} \text{Var}(\hat{L}_i) &= w_d^\top \text{Cov}(\hat{L}_{d-1,i}) w_d, \\ \Leftrightarrow \frac{\text{Var}(\hat{L}_i)}{n_b} &= w_d^\top \frac{\text{Cov}(\hat{L}_{d-1,i})}{n_b} w_d \leq \|w_d\| \times \left\| \text{Cov} \left(\frac{\partial \hat{L}_b(D, G)}{\partial w_d} \right) w_d \right\|, \\ \Rightarrow \frac{\text{Var}(\hat{L}_b(D, G))}{\|w_d\|^2} &\leq \left\| \text{Cov} \left(\frac{\partial \hat{L}_b(D, G)}{\partial w_d} \right) w_d \right\| / \|w_d\|. \end{aligned}$$

by the Cauchy–Schwarz inequality, where $\text{Var}(\hat{L}_b(D, G)) = \text{Var}(\hat{L}_i)/n_b$ and $\text{Cov}(\partial \hat{L}_b(D, G)/\partial w_d) = \text{Cov}(\hat{L}_{d-1,i})/n_b$ with $n_b = m_b$. Therefore, by applying the definition of the induced norm to the right-hand side, we obtain the result. \square

Lemma 2. Define $\delta_t^\epsilon = P(L_i^{(t)} \leq \epsilon)$, $\mu_{\mathcal{S}_t} = \mathbf{E}(L_i^{(t)} | L_i^{(t)} \leq \epsilon)$ and $\sigma_{\mathcal{S}_t}^2 = \text{Var}(L_i^{(t)} | L_i^{(t)} \leq \epsilon)$. The variance of $L_i^{(t)}$ is bounded below by

$$\text{Var}(L_i^{(t)}) \geq \delta_t^\epsilon \sigma_{\mathcal{S}_t}^2 + \delta_t^\epsilon (1 - \delta_t^\epsilon) (\mathbf{E}(L_i^{(t)} | L_i^{(t)} \geq \epsilon) - \mu_{\mathcal{S}_t})^2.$$

Proof. Recall $L_i^{(t)} = D^{(t)}(X_i) - \mathbf{E}[D^{(t)}(G^{(t)}(Z))]$ and $\delta_t^\epsilon = P(L_i^{(t)} \leq \epsilon)$. Let's denote by A the classification rule such that $A_1 : \{L_i^{(t)} \leq \epsilon\}$ and $A_2 : \{L_i^{(t)} > \epsilon\}$. We define $\mu_{\mathcal{S}_t} = \mathbf{E}(L_i^{(t)} | A_1)$ and $\sigma_{\mathcal{S}_t}^2 = \text{Var}(L_i^{(t)} | A_1)$. Then, by the Jensen's inequality, we have

$$\mathbf{E}(\text{Var}(L_i^{(t)} | A)) = \delta_t^\epsilon \text{Var}(L_i^{(t)} | A_1) + (1 - \delta_t^\epsilon) \text{Var}(L_i^{(t)} | A_2) \geq \delta_t^\epsilon \sigma_{\mathcal{S}_t}^2.$$

On the one hand,

$$\begin{aligned} \text{Var}(\mathbf{E}(L_i^{(t)} | A)) &= \delta_t^\epsilon (1 - \delta_t^\epsilon)^2 (\mu_{\mathcal{S}_t} - \mathbf{E}(L_i^{(t)} | A_2))^2 + \delta_t^{\epsilon^2} (1 - \delta_t^\epsilon) (\mu_{\mathcal{S}_t} - \mathbf{E}(L_i^{(t)} | A_2))^2, \\ &= \delta_t^\epsilon (1 - \delta_t^\epsilon) (\mathbf{E}(L_i^{(t)} | A_2) - \mu_{\mathcal{S}_t})^2. \end{aligned}$$

Therefore,

$$\begin{aligned} \text{Var}(L_i^{(t)}) &= \mathbf{E}(\text{Var}(L_i^{(t)} | A)) + \text{Var}(\mathbf{E}(L_i^{(t)} | A)), \\ &\geq \delta_t^\epsilon \sigma_{\mathcal{S}_t}^2 + \delta_t^\epsilon (1 - \delta_t^\epsilon) (\mathbf{E}(L_i^{(t)} | A_2) - \mu_{\mathcal{S}_t})^2. \end{aligned}$$

□

Suppose $\|w_d^{(t)}\| > 0$. Let $\delta_t^\epsilon = P(L_i^{(t)} \leq \epsilon)$, $\sigma_{\mathcal{S}_t}^2 = \text{Var}(L_i^{(t)} | L_i^{(t)} \leq \epsilon)$, $\sigma_{G^{(t)}}^2 = \text{Var}(D^{(t)}(G^{(t)}(Z_j)))$, and $\mathbf{E}(L_i^{(t)} | L_i^{(t)} \leq \epsilon) = 0$ for some $\epsilon > 0$. Then, by combining Lemmas 1 and 2, the variance of $\hat{L}_b(D^{(t)}, G^{(t)})$ is bounded below

$$\begin{aligned} \text{Var}(\hat{L}_b(D^{(t)}, G^{(t)})) &= \text{Var}\left(\frac{1}{n_b} \sum_{i=1}^{n_b} L_i^{(t)}\right) \\ &\quad + \text{Var}\left(\frac{1}{m_b} \sum_{j=1}^{m_b} (\mathbf{E}(D^{(t)}(G^{(t)}(Z_j))) - D^{(t)}(G^{(t)}(Z_j)))\right), \\ &\geq \frac{1}{n_b} \left(\delta_\epsilon \sigma_{\mathcal{S}_t}^2 + \delta_t^\epsilon (1 - \delta_t^\epsilon) \mathbf{E}(L_i^{(t)} | A_2)^2\right) + \frac{\sigma_{G^{(t)}}^2}{m_b}. \end{aligned}$$

B.3 Theorem 1

The main theorem is predicated on the following two lemmas. All the proof assumes that all minibatches consist of independent samples.

Lemma 3. Under (A1-3), for any $D \in \mathcal{D}$ and $G \in \mathcal{G}$,

$$|\hat{L}_b(D, G)| \leq d_{\mathcal{D}}(p_X, p_{G(Z)}) + O_p(1/\sqrt{n_b}).$$

Proof. Since the support is compact, $D(\cdot)$ is bounded. Let $L_i = D(X_i) - D(G(Z_i))$ and denote by $L = E(L_i)$. Since $|\hat{L}_b - L| \geq ||\hat{L}_b| - |L||$,

$$P(|\hat{L}_b| - |L| \geq C) \leq P(|\hat{L}_b - L| \geq C) \leq \frac{\text{Var}(\hat{L}_b)}{C^2} = \frac{\text{Var}(D(X_i)) + \text{Var}(D(G(Z_i)))}{n_b C^2},$$

for some $C > 0$. By the Chebyshev's inequality, $|\hat{L}_b| = |L| + O_p(1/\sqrt{n_b})$. Since $|L| \leq d_{\mathcal{D}}(p_X, p_{G(Z)})$, we obtain the result. □

Lemma 4. Under (A1-3), let's define $\hat{L}_l(D, G^{(t)}) = \sum_{i=1}^{n_b} D_l(X_i)/n_b - \sum_{j=1}^{m_b} D_l(G^{(t)}(Z_j))/m_b$ where D_l denote the output of the l th hidden layer of D . Denote by $\hat{L}_{l,i}$ the i th node in the hidden layer. Then $|\hat{L}_{l,i}| \leq d_{\mathcal{D}}(p_X, p_{G^{(t)}}) + O_p(1/\sqrt{n_b})$ for all $i = 1, \dots, p_{l+1}$ and $l = 1, \dots, d-1$.

Proof. For $l = d - 1$, the conclusion is trivial, so we consider $l = d - 2$. Considering \mathcal{D} is a symmetric family (i.e., if $D \in \mathcal{D}$, then $-D \in \mathcal{D}$), the optimal critic with $G^{(t)}$ is obtained by

$$\begin{aligned}
\hat{D}_t^* &= \arg_{D \in \mathcal{D}} \max \hat{L}_b(D, G^{(t)}), \\
&= \arg_{D \in \mathcal{D}} \max \left| \frac{1}{n_b} \sum_{i=1}^{n_b} D(X_i) - \frac{1}{m_b} \sum_{j=1}^{m_b} D(G^{(t)}(Z_j)) \right|, \\
&= \arg_{D \in \mathcal{D}} \max \left| \frac{1}{n_b} \sum_{i=1}^{n_b} w_d^\top D_{d-1}(X_i) - \frac{1}{m_b} \sum_{j=1}^{m_b} w_d^\top D_{d-1}(G^{(t)}(Z_j)) \right|, \\
&= \arg_{D \in \mathcal{D}} \max \left| w_d^\top \hat{L}_{d-1}(D, G^{(t)}) \right|.
\end{aligned}$$

Because of the update procedure of the critic, it follows $|\hat{w}_d^{*\top} \hat{L}_{d-1}| \geq |w_d^\top \hat{L}_{d-1}|$ for any other w_d where \hat{w}_d^* achieves the maximum. Let's define $\mathbf{0}_{-i} = (0, \dots, 1, \dots, 0)^\top$ where the i th element is 1 but 0 otherwise. Then, we see $|\hat{w}_d^{*\top} \hat{L}_{d-1}| \geq |\mathbf{0}_{-i}^\top \hat{L}_{d-1}| = |\hat{L}_{d-1,i}|$ for all i where $\hat{L}_{d-1,i}$ is the i th hidden node in its output layer. Therefore, we obtain $|\hat{L}_{d-1,i}(D, G^{(t)})| \leq \hat{L}_b(\hat{D}_t^*, G^{(t)})$ for all i and for any $D \in \mathcal{D}$. By the way, the same proof technique holds for other $l = 1, \dots, d - 3$. Therefore, we obtain $|\hat{L}_{l,i}(D^{(t)}, G^{(t)})| \leq \hat{L}_b(\hat{D}_t^*, G^{(t)})$ for all $i = 1, \dots, p_{l+1}$ and $l = 1, \dots, d - 1$. By Lemma 3, we conclude the shown result. \square

To prove the main theorem, let's denote by \hat{L}_l the output of the l th hidden layer while \hat{F}_l the output of its layer before passing the activation function. For instance, if $l = d - 1$,

$$\begin{aligned}
\hat{L}_d &= w_d^\top \hat{L}_{d-1} \\
\hat{L}_{d-1} &= \frac{1}{n_b} \sum_{i=1}^{n_b} D_{d-1}(X_i) - \frac{1}{m_b} \sum_{j=1}^{m_b} D_{d-1}(G(Z_j)) \\
\hat{F}_{d-1} &= \frac{1}{n_b} \sum_{i=1}^{n_b} W_{d-1} D_{d-2}(X_i) - \frac{1}{m_b} \sum_{j=1}^{m_b} W_{d-1} D_{d-1}(G(Z_j)), \\
&= W_{d-1} \hat{L}_{d-2}.
\end{aligned}$$

Let's denote by $W_{l,i,j}$ the (i, j) th element and $W_{l,i}$, the i th row vector of W_l . The backprop-

agation system induces

$$\begin{aligned}
\frac{\partial \hat{L}_d}{\partial w_{d,j}} &= \hat{L}_{d-1,j}, \\
\frac{\partial \hat{L}_d}{\partial W_{d-1,i,j}} &= \frac{\partial \hat{L}_d}{\partial \hat{L}_{d-1,j}} \frac{\partial \hat{L}_{d-1,j}}{\partial \hat{F}_{d-1,j}} \frac{\partial \hat{F}_{d-1,j}}{\partial W_{d-1,i,j}}, \\
\frac{\partial \hat{L}_d}{\partial W_{d-2,i,j}} &= \frac{\partial \hat{L}_d}{\partial \hat{L}_{d-1}} \frac{\partial \hat{L}_{d-1}}{\partial \hat{F}_{d-1}} \frac{\partial \hat{F}_{d-1}}{\partial \hat{L}_{d-2,j}} \frac{\partial \hat{L}_{d-2,j}}{\partial \hat{F}_{d-2,j}} \frac{\partial \hat{F}_{d-2,j}}{\partial W_{d-2,i,j}}, \\
\frac{\partial \hat{L}_d}{\partial W_{d-3,i,j}} &= \frac{\partial \hat{L}_d}{\partial \hat{L}_{d-1}} \frac{\partial \hat{L}_{d-1}}{\partial \hat{F}_{d-1}} \frac{\partial \hat{F}_{d-1}}{\partial \hat{L}_{d-2}} \frac{\partial \hat{L}_{d-2}}{\partial \hat{F}_{d-2}} \frac{\partial \hat{F}_{d-2}}{\partial \hat{L}_{d-3,j}} \frac{\partial \hat{L}_{d-3,j}}{\partial \hat{F}_{d-3,j}} \frac{\partial \hat{F}_{d-3,j}}{\partial W_{d-3,i,j}}, \\
&\vdots \\
\frac{\partial \hat{L}_d}{\partial W_{1,i,j}} &= \frac{\partial \hat{L}_d}{\partial \hat{L}_{d-1}} \cdots \frac{\partial \hat{F}_{1,j}}{\partial W_{1,i,j}}.
\end{aligned}$$

Let's denote by K_l^\dagger the diagonal matrix whose element is $\partial \hat{L}_l / \partial \hat{F}_l$. Each element amounts to at most $K_\kappa(l)$. In other words,

$$\begin{aligned}
\frac{\partial \hat{L}_d}{\partial w_{d,j}} &= \hat{L}_{d-1,j}, \\
\frac{\partial \hat{L}_d}{\partial W_{d-1,i,j}} &= w_{d,j} K_{d-1,j,j}^\dagger \hat{L}_{d-2,i}, \\
\frac{\partial \hat{L}_d}{\partial W_{d-2,i,j}} &= w_d \cdot K_{d-1}^\dagger \cdot W_{d-1,j} \cdot K_{d-2,j,j}^\dagger \hat{L}_{d-3,i}, \\
\frac{\partial \hat{L}_d}{\partial W_{d-3,i,j}} &= w_d \cdot K_{d-1}^\dagger \cdot W_{d-1} \cdot K_{d-2}^\dagger \cdot W_{d-2,j} K_{d-3,j,j}^\dagger \hat{L}_{d-4,i}, \\
&\vdots
\end{aligned}$$

so, by Lemma 4,

$$\begin{aligned}
\left| \frac{\partial \hat{L}_d}{\partial w_{d,j}} \right| &= \left| \hat{L}_{d-1,j} \right| \leq d_{\mathcal{D}}(p_X, p_{G^{(t)}}) + O_p(1/\sqrt{n_b}), \\
\left| \frac{\partial \hat{L}_d}{\partial W_{d-1,i,j}} \right| &= |w_{d,j} K_{d-1,j}^\dagger \hat{L}_{d-2,i}| \leq M_w(d) K_\kappa(d-1) |\hat{L}_{d-2,i}|, \\
&\leq M_w(d) K_\kappa(d-1) d_{\mathcal{D}} + O_p(1/\sqrt{n_b}), \\
\left| \frac{\partial \hat{L}_d}{\partial W_{d-2,i,j}} \right| &= |w_d K_{d-1}^\dagger \cdot W_{d-1,j} \cdot K_{d-2,j,j}^\dagger \hat{L}_{d-3,i}|, \\
&\leq \|w_d\| \times \|K_{d-1}^\dagger\|_F \times \|W_{d-1,j}\| \times K_\kappa(d-2) \times |\hat{L}_{d-3,i}|, \\
&\leq M_w(d) \sqrt{p_{d-1}} K_\kappa(d-1) M_w(d-1) K_\kappa(d-2) |\hat{L}_{d-3,i}|, \\
&\leq \sqrt{p_{d-1}} \prod_{l=d-1}^d M_w(l) \prod_{s=d-2}^{d-1} K_\kappa(s) d_{\mathcal{D}} + O_p(1/\sqrt{n_b}).
\end{aligned}$$

In the same manner, we obtain

$$\left| \frac{\partial \hat{L}_d}{\partial W_{k,i,j}} \right| \leq \prod_{t=k+1}^{d-1} \sqrt{p_t} \prod_{l=k+1}^d M_w(l) \prod_{s=k}^{d-1} K_\kappa(s) d_{\mathcal{D}} + O_p(1/\sqrt{n_b}),$$

for $k = 1, \dots, d-2$.

B.4 Corollary 1

Recall $C_{w,\kappa}(k) = \prod_{l=k+1}^d \sqrt{p_l} M_w^{(t)}(l) \prod_{s=k}^{d-1} K_\kappa(s)$ for $k = 1, \dots, d-2$, $C_{w,\kappa}(d-1) = M_w(d) K_\kappa(d-1)$, and $C_{w,\kappa}(d) = 1$. By the direct result of Theorem 1,

$$\left| \frac{\partial \hat{L}_b^\alpha(D^{(t)}, G^{(t)})}{\partial W_{k,i,j}^{(t)}} \right| \leq C_{w,\kappa}(k) d_{\mathcal{D}}(p_{Q^{\alpha,\alpha}}, p_{G^{(t)}(Z^{\alpha,\alpha}, \alpha)}) + O_p\left(\frac{1}{\sqrt{n_b}}\right), \quad (12)$$

for $k = 1, \dots, d$.

Considering $\mathbf{E}_{Q^{\alpha,\alpha}} = \mathbf{E}_\alpha \mathbf{E}_{Q^\alpha|\alpha}$, the use of $\alpha \sim r\delta_1 + (1-r)p_{\alpha^*}$ makes the joint neural

distance upper bound

$$\begin{aligned}
& d_{\mathcal{D}}(p_{Q^{\alpha}, \alpha}, p_{G^{(t)}(Z^{\alpha}, \alpha), \alpha}) \\
& := \sup_D \int D(q_a, a) p(q_a | a) p(a) dq_a da - \int D(G(z_a, a), a) p(G(z_a, a) | a) p(a) dz_a da \\
& \leq r \left(\sup_D \int_{a=1} D(x, 1) p(x) dx - \int_{a=1} D(G(z, 1), 1) p(G(z)) dz \right) \\
& + (1-r) \left(\sup_D \int_{a \neq 1} D(q_a^*, a^*) p(q_a^*, a^*) dq_a^* da^* - \int_{a \neq 1} D(G(z_a^*, a^*), a^*) p(G(z_a^*, a^*), a^*) dz_a^* da^* \right), \\
& := r d_{\mathcal{D}}(p_{X, 1}, p_{G^{(t)}(Z, 1), 1}) + (1-r) d_{\mathcal{D}}(p_{Q^{\alpha^*}, \alpha^*}, p_{G^{(t)}(Z^{\alpha^*}, \alpha^*), \alpha^*}).
\end{aligned}$$

Hence, the condition in the statement is obtained.

B.5 Theorem 2

Theorem 2 is the direct result of combining Lemmas 5 and 6 that appear below.

Let's denote by $\mathcal{R}(\mathcal{F})$ the Rademacher complexity of a generic function class \mathcal{F} . For i.i.d. $X_1, \dots, X_n \sim p_X$, the quantity is defined as $\mathcal{R}(\mathcal{F}) = \mathbf{E}_{X_1, \dots, X_n, \epsilon} \left[\sup_{f \in \mathcal{F}} \left| \frac{1}{n} \sum_{i=1}^n \epsilon_i f(X_i) \right| \right]$ where $\epsilon_1, \dots, \epsilon_n \sim \text{Unif}\{-1, 1\}$ i.i.d. Lemma 5 quantifies this statistical quantity based on the Rademacher complexity \mathcal{R} . The derived bound explicitly relates to the parameters of \mathcal{D} and \mathcal{G} . For further analysis, we define the composite function class of $\mathcal{O} = \{D(G(z, a), a) : z \in \mathbb{R}^{dz}, a \in [0, 1], D \in \mathcal{D}, G \in \mathcal{G}\}$.

Lemma 5. Under (A1-3), let $\hat{G}^* = \arg_{G \in \mathcal{G}} \min d_{\mathcal{D}}(\hat{p}_{Q^{\alpha}, \alpha}, \hat{p}_{G(Z^{\alpha}, \alpha), \alpha})$. With $1 - 2\delta$ probability, the estimation error is bounded above by

$$\begin{aligned}
& d_{\mathcal{D}}(p_{Q^{\alpha}, \alpha}, p_{\hat{G}^*(Z^{\alpha}, \alpha), \alpha}) - \inf_{G \in \mathcal{G}} d_{\mathcal{D}}(p_{Q^{\alpha}, \alpha}, p_{G(Z^{\alpha}, \alpha), \alpha}) \\
& \leq 4(\mathcal{R}(\mathcal{D}) + \mathcal{R}(\mathcal{O})) + C_{B_X, B_{\alpha}, \mathbf{w}, \kappa} \sqrt{\frac{\log(1/\delta)}{n_e}} + C_{B_Z, B_{\alpha}, \mathbf{v}, \mathbf{w}, \psi, \kappa} \sqrt{\frac{\log(1/\delta)}{m}}, \quad (13)
\end{aligned}$$

where $C_{B_X, B_{\alpha}, \mathbf{w}, \kappa}$ and $C_{B_Z, B_{\alpha}, \mathbf{v}, \mathbf{w}, \psi, \kappa}$ are specified in the below proof.

Proof. Following the proof of Theorem 1 in Ji et al. (2021), the estimation error is decomposed as follows

$$\begin{aligned} d_{\mathcal{D}}(p_{Q^{\alpha},\alpha}, p_{\hat{G}^*(Z^{\alpha},\alpha),\alpha}) - \inf_G d_{\mathcal{D}}(p_{Q^{\alpha},\alpha}, p_{G(Z^{\alpha},\alpha),\alpha}) \\ = d_{\mathcal{D}}(p_{Q^{\alpha},\alpha}, p_{\hat{G}^*(Z^{\alpha},\alpha),\alpha}) - d_{\mathcal{D}}(\hat{p}_{Q^{\alpha},\alpha}, p_{\hat{G}^*(Z^{\alpha},\alpha),\alpha}) \end{aligned} \quad (14)$$

$$+ \inf_G d_{\mathcal{D}}(\hat{p}_{Q^{\alpha},\alpha}, p_{G(Z^{\alpha},\alpha),\alpha}) - \inf_G d_{\mathcal{D}}(p_{Q^{\alpha},\alpha}, p_{G(Z^{\alpha},\alpha),\alpha}) \quad (15)$$

$$+ d_{\mathcal{D}}(\hat{p}_{Q^{\alpha},\alpha}, p_{\hat{G}^*(Z^{\alpha},\alpha),\alpha}) - \inf_G d_{\mathcal{D}}(\hat{p}_{Q^{\alpha},\alpha}, p_{G(Z^{\alpha},\alpha),\alpha}). \quad (16)$$

Then (14) and (15) have the upper bound

$$(14), (15) \leq \sup_D |\mathbf{E}D(Q^{\alpha}, \alpha) - \hat{\mathbf{E}}D(Q^{\alpha}, \alpha)|,$$

where $\hat{\mathbf{E}}$ implies the expectation over the empirical mass function. Let's denote $\tilde{G} = \arg_G \min d_{\mathcal{D}}(\hat{p}_{Q^{\alpha},\alpha}, p_{G(Z^{\alpha},\alpha),\alpha})$. Then (16) is bounded above by

$$\begin{aligned} (16) &= d_{\mathcal{D}}(\hat{p}_{Q^{\alpha},\alpha}, p_{\hat{G}^*(Z^{\alpha},\alpha),\alpha}) - d_{\mathcal{D}}(\hat{p}_{Q^{\alpha},\alpha}, \hat{p}_{\hat{G}^*(Z^{\alpha},\alpha),\alpha}) + d_{\mathcal{D}}(\hat{p}_{Q^{\alpha},\alpha}, \hat{p}_{\hat{G}^*(Z^{\alpha},\alpha),\alpha}) - d_{\mathcal{D}}(\hat{p}_{Q^{\alpha},\alpha}, p_{\tilde{G}(Z^{\alpha},\alpha),\alpha}), \\ &\leq d_{\mathcal{D}}(\hat{p}_{Q^{\alpha},\alpha}, p_{\hat{G}^*(Z^{\alpha},\alpha),\alpha}) - d_{\mathcal{D}}(\hat{p}_{Q^{\alpha},\alpha}, \hat{p}_{\hat{G}^*(Z^{\alpha},\alpha),\alpha}) + d_{\mathcal{D}}(\hat{p}_{Q^{\alpha},\alpha}, \hat{p}_{\tilde{G}(Z^{\alpha},\alpha),\alpha}) - d_{\mathcal{D}}(\hat{p}_{Q^{\alpha},\alpha}, p_{\tilde{G}(Z^{\alpha},\alpha),\alpha}), \\ &\leq 2 \sup_{D,G} |\mathbf{E}D(G(Z^{\alpha}, \alpha), \alpha) - \hat{\mathbf{E}}D(G(Z^{\alpha}, \alpha), \alpha)|. \end{aligned}$$

Let $U_1((Q_1^{\alpha_1}, \alpha_1), \dots, (Q_n^{\alpha_{n_e}}, \alpha_{n_e})) = \sup_D |\mathbf{E}D(Q^{\alpha}, \alpha) - \hat{\mathbf{E}}D(Q^{\alpha}, \alpha)|$. To apply the McDiarmid's inequality, we first check whether or not U_1 satisfies a bounded difference. We denote by $(\tilde{Q}_j^{\tilde{\alpha}_j}, \tilde{\alpha}_j)$ the j th random vector independent to $(Q_j^{\alpha_j}, \alpha_j)$. Then

$$\begin{aligned} |U_1((Q_1^{\alpha_1}, \alpha_1), \dots, (Q_j^{\alpha_j}, \alpha_j), \dots, (Q_n^{\alpha_{n_e}}, \alpha_{n_e})) - U_1((Q_1^{\alpha_1}, \alpha_1), \dots, (\tilde{Q}_j^{\tilde{\alpha}_j}, \tilde{\alpha}_j), \dots, (Q_n^{\alpha_{n_e}}, \alpha_{n_e}))| \\ \leq \frac{1}{n_e} \sup_{\mathbf{w}} |D(Q_j^{\alpha_j}, \alpha_j) - D(\tilde{Q}_j^{\tilde{\alpha}_j}, \tilde{\alpha}_j)|, \\ \leq \frac{1}{n_e} \prod_{l=1}^d M_w(l) \times \prod_{s=1}^{d-1} K_{\kappa}(s) \times \|[Q_j - Q'_j, \alpha_j - \alpha'_j]\|, \\ \leq \frac{1}{n_e} \prod_{l=1}^d M_w(l) \times \prod_{s=1}^{d-1} K_{\kappa}(s) \times \sqrt{2B_X^2 + 2B_{\alpha}^2} = \frac{\sqrt{2}}{n_e} C_{B_X, B_{\alpha}, \mathbf{w}, \kappa}, \end{aligned}$$

where the second inequality comes from the Cauchy-Schwarz inequality and Lipschitz activation functions. Next, the expectation of U_1 is

$$\begin{aligned}
\mathbf{E}_{Q,\alpha} U_1 &\leq \mathbf{E}_{Q,\alpha,\tilde{Q},\tilde{\alpha}} \sup_D \left| \frac{1}{n_e} \sum_{j=1}^{n_e} D(\tilde{Q}_j^{\alpha_j}, \tilde{\alpha}_j) - D(Q_j^{\alpha_j}, \alpha_j) \right|, \\
&\leq \mathbf{E}_{Q,\alpha,\tilde{Q},\tilde{\alpha},\epsilon} \sup_D \left| \frac{1}{n_e} \sum_{j=1}^{n_e} \epsilon_j (D(\tilde{Q}_j^{\alpha_j}, \tilde{\alpha}_j) - D(Q_j^{\alpha_j}, \alpha_j)) \right|, \\
&\leq 2\mathbf{E}_{Q,\alpha,\tilde{Q},\tilde{\alpha},\epsilon} \sup_D \left| \frac{1}{n_e} \sum_{j=1}^{n_e} \epsilon_j D(Q_j^{\alpha_j}, \alpha_j) \right| = 2\mathcal{R}(\mathcal{D}).
\end{aligned}$$

Therefore, by the McDiarmid's inequality, (14) upper bounds

$$(14) \leq 2\mathcal{R}(\mathcal{D}) + C_{B_X, B_\alpha, \mathbf{v}, \psi} \sqrt{\frac{\log(1/\delta)}{n_e}},$$

with $1-\delta$ probability. Now, let $U_2(Z_1^\alpha, \dots, Z_m^\alpha) = \sup_{D,G} |\mathbf{E}D(G(Z^\alpha, \alpha), \alpha) - \hat{\mathbf{E}}D(G(Z^\alpha, \alpha), \alpha)|$.

U_2 satisfies a bounded difference as a result of the Cauchy-Schwarz inequality, i.e.,

$$\begin{aligned}
&|U_2((Z^{\alpha_1}, \alpha_1), \dots, (Z^{\alpha_j}, \alpha_j), \dots, (Z^{\alpha_m}, \alpha_m)) - U_2((Z^{\alpha_1}, \alpha_1), \dots, (\tilde{Z}^{\tilde{\alpha}_j}, \tilde{\alpha}_j), \dots, (Z^{\alpha_m}, \alpha_m))| \\
&\leq \frac{1}{m} \sup_{D,G} |D(G(Z^{\alpha_j}, \alpha_j), \alpha_j) - D(G(\tilde{Z}^{\tilde{\alpha}_j}, \tilde{\alpha}_j), \tilde{\alpha}_j)|, \\
&\leq \frac{1}{m} \prod_{l=1}^d M_w(l) \prod_{s=1}^{d-1} K_\kappa(s) \times \|[G(Z_j^{\alpha_j}, \alpha_j), \alpha_j] - [G(\tilde{Z}_j^{\tilde{\alpha}_j}, \tilde{\alpha}_j), \tilde{\alpha}_j]\|, \\
&= \frac{1}{m} \prod_{l=1}^d M_w(l) \prod_{s=1}^{d-1} K_\kappa(s) \times \sqrt{\|G(Z_j^{\alpha_j}, \alpha_j) - G(\tilde{Z}_j^{\tilde{\alpha}_j}, \tilde{\alpha}_j)\|^2 + \|\alpha_j - \tilde{\alpha}_j\|^2}, \\
&\leq \frac{1}{m} \prod_{l=1}^d M_w(l) \prod_{s=1}^{d-1} K_\kappa(s) \times (\|G(Z_j^{\alpha_j}, \alpha_j) - G(\tilde{Z}_j^{\tilde{\alpha}_j}, \tilde{\alpha}_j)\| + \|\alpha_j - \tilde{\alpha}_j\|), \\
&\leq \frac{1}{m} \prod_{l=1}^d M_w(l) \prod_{s=1}^{d-1} K_\kappa(s) \times \left(\prod_{l=1}^g M_v(l) \prod_{s=1}^{g-1} K_\psi(s) \sqrt{\|Z_j^{\alpha_j} - \tilde{Z}_j^{\tilde{\alpha}_j}\|^2 + \|\alpha_j - \tilde{\alpha}_j\|^2 + 2B_\alpha} \right), \\
&\leq \frac{1}{m} \prod_{l=1}^d M_w(l) \prod_{s=1}^{d-1} K_\kappa(s) \times \left(\prod_{l=1}^g M_v(l) \prod_{s=1}^{g-1} K_\psi(s) \sqrt{2B_Z^2 + 2B_\alpha^2 + 2B_\alpha} \right), \\
&\leq \frac{\sqrt{2}}{m} \prod_{l=1}^d M_w(l) \prod_{s=1}^{d-1} K_\kappa(s) \times \left(\prod_{l=1}^g M_v(l) \prod_{s=1}^{g-1} K_\psi(s) \sqrt{B_Z^2 + B_\alpha^2 + \sqrt{2}B_\alpha} \right), \\
&= \frac{\sqrt{2}}{m} C_{B_Z, B_\alpha, \mathbf{v}, \psi, \kappa}.
\end{aligned}$$

Then the expectation of U_2 is

$$\begin{aligned}
\mathbf{E}_{Z,\alpha} U_2 &\leq \mathbf{E}_{Z,\alpha,\tilde{Z},\tilde{\alpha}} \sup_{D,G} \left| \frac{1}{m} \sum_{j=1}^m D(G(\tilde{Z}_j^{\tilde{\alpha}}, \tilde{\alpha}_j), \tilde{\alpha}_j) - D(G(Z_j^\alpha, \alpha_j), \alpha_j) \right|, \\
&\leq \mathbf{E}_{Z,\alpha,\tilde{Z},\tilde{\alpha},\epsilon} \sup_{D,G} \left| \frac{1}{m} \sum_{j=1}^m \epsilon_j (D(G(\tilde{Z}_j^{\tilde{\alpha}}, \tilde{\alpha}_j), \tilde{\alpha}_j) - D(G(Z_j^{\alpha_j}, \alpha_j), \alpha_j)) \right|, \\
&\leq 2 \mathbf{E}_{Z,\alpha,\tilde{Z},\tilde{\alpha},\epsilon} \sup_{D,G} \left| \frac{1}{m} \sum_{j=1}^m \epsilon_j D(G(Z_j^{\alpha_j}, \alpha_j), \alpha_j) \right| = 2\mathcal{R}(\mathcal{O}).
\end{aligned}$$

Therefore, (16) upper bounds

$$(16) \leq 2 \times \left(2\mathcal{R}(\mathcal{O}) + C_{B_Z, B_\alpha, \mathbf{v}, \mathbf{w}, \psi, \kappa} \sqrt{\frac{\log(1/\delta)}{m}} \right),$$

with $1 - \delta$ probability by the McDiarmid's inequality. By combining the above upper bounds, we have result in the statement. \square

Lemma 6. Under (A1-4), the Rademacher complexities are further bounded

$$\begin{aligned}
\mathcal{R}(\mathcal{D}) &\leq \frac{\sqrt{B_X^2 + 1} \prod_{l=1}^d M_w(l) \prod_{s=1}^{d-1} K_\psi(s) \sqrt{3d}}{\sqrt{n_e}}, \\
\mathcal{R}(\mathcal{O}) &\leq \frac{\sqrt{B_Z^2 + 1} \prod_{l=1}^g M_v(l) \prod_{s=1}^{g-1} K_\kappa(s) \times \prod_{l=1}^d M_w(l) \prod_{s=1}^{d-1} K_\psi(s) \sqrt{3(g+d-1)}}{\sqrt{m}}.
\end{aligned}$$

Proof. By Theorem 1 in Golowich et al. (2018), the Rademacher complexity of \mathcal{D} upper bounds

$$\begin{aligned}
\mathcal{R}(\mathcal{D}) &\leq \frac{\| [Q_j^{\alpha_j}, \alpha_j] \| \prod_{l=1}^d M_w(l) \prod_{s=1}^{d-1} K_\psi(s) (\sqrt{2d \log 2} + 1)}{\sqrt{n_e}}, \\
&\leq \frac{\sqrt{B_X^2 + 1} \prod_{l=1}^d M_w(l) \prod_{s=1}^{d-1} K_\psi(s) \sqrt{3d}}{\sqrt{n_e}},
\end{aligned}$$

because of $\sqrt{2d \log 2} + 1 \leq \sqrt{3d}$. Similarly, for \mathcal{O} , we have

$$\begin{aligned}
\mathcal{R}(\mathcal{O}) &\leq \frac{\| [G(Z_j^{\alpha_j}, \alpha_j), \alpha_j] \| \prod_{l=1}^d M_w(l) \prod_{s=1}^{d-1} K_\psi(s) \sqrt{3d}}{\sqrt{m}}, \\
&\leq \frac{\| [G(Z_j^{\alpha_j}, \alpha_j), \alpha_j] \| \prod_{l=1}^d M_w(l) \prod_{s=1}^{d-1} K_\psi(s) \sqrt{3d}}{\sqrt{m}} + \frac{1 \times \prod_{l=1}^d M_w(l) \prod_{s=1}^{d-1} K_\psi(s) \sqrt{3d}}{\sqrt{m}}, \\
&\leq \frac{\sqrt{B_Z^2 + 1} \prod_{l=1}^g M_v(l) \prod_{s=1}^{g-1} K_\kappa(s) \times \prod_{l=1}^d M_w(l) \prod_{s=1}^{d-1} K_\psi(s) \sqrt{3(g+d-1)}}{\sqrt{m}} \\
&\quad + \frac{B_\alpha \prod_{l=1}^d M_w(l) \prod_{s=1}^{d-1} K_\psi(s) \sqrt{3d}}{\sqrt{m}}, \\
&= \frac{\prod_{l=1}^d M_w(l) \prod_{s=1}^{d-1} K_\psi(s)}{\sqrt{m}} \left(\sqrt{B_Z^2 + 1} \prod_{l=1}^g M_v(l) \prod_{s=1}^{g-1} K_\kappa(s) \sqrt{3(g+d-1)} + 1 \times \sqrt{3d} \right).
\end{aligned}$$

Note the term $(g+d-1)$ conceptually stands for the depth of the composite neural network, so it stems from the part $\|W_1 V_g\|_F \leq M_w(1) M_v(g)$.

Therefore, by assuming that \mathcal{G} is sufficiently large such that $p_{Q^\alpha, \alpha} \in \mathcal{P}_{\mathcal{G}, \alpha}$ and the number m of samples drawn from the distribution p_z scales faster than n_e , we obtain the result. \square

B.6 Theorem 3

We introduce the Fano's lemma in Ji et al. (2021).

Lemma (Fano's Lemma). For $M \geq 2$, assume that there exists M hypotheses $\theta_0, \dots, \theta_M \in \Theta$ satisfying (i) $d(\theta_i, \theta_j) \geq 2s > 0$ for all $0 \leq i < j \leq M$; (ii) $\frac{1}{M} \sum_{i=1}^M KL(P_{\theta_i} \| P_{\theta_0}) \leq \alpha \log M$, $0 < \alpha \leq 1/8$, where $d(\cdot, \cdot)$ is a semi-distance and P_θ is a probability measure with respect to the randomness of data D . Then, we have

$$\inf_{\hat{\theta}} \sup_{\theta \in \Theta} P_{D \sim P_\theta} [d(\hat{\theta}, \theta) \geq s] \geq \frac{\sqrt{M}}{1 + \sqrt{M}} \left(1 - 2\alpha - \frac{2\alpha}{\log M} \right).$$

Now, let's consider the following hypothetical distribution

$$p_u(q, \alpha) = \begin{cases} 1/4 - u\delta_{q,a}, & \text{if } q = q_1, \alpha = 1, \\ 1/4 + u\delta_{q,a}, & \text{if } q = -q_1, \alpha = 1, \\ 1/4 - u\delta_{q,a}, & \text{if } q = q_1, \alpha = 0, \\ 1/4 + u\delta_{q,a}, & \text{if } q = -q_1, \alpha = 0, \end{cases}$$

where $\|q_1\| = B_X$ for $q_1, -q_1 \in \mathcal{Q}$.

The (l, k) th element of W_i for $1 \leq i < d$ is denoted by $W_{i,l,k}$. The k th column vector of the i th layer is denoted by $W_{i,\cdot,k}$. The final layer w_d is a $p_d \times 1$ vector, and $w_{d,l}$ denotes the l th element. We select $\mathbf{w}^\dagger \in \mathbf{W}$ such that $w_{d,1}^\dagger = M_w(d)$, $w_{d,l}^\dagger = 0$ for $l \neq 1$, $W_{i,1,1}^\dagger = M_w(i)$ for $2 \leq i \leq d-1$, $W_{i,l,k}^\dagger = 0$ for $(l, k) \neq (1, 1)$, $W_{1,\cdot,1}^\dagger = M_w(1) \frac{\tilde{q}}{\|\tilde{q}\|}$, and $W_{1,\cdot,l}^\dagger = \mathbf{0}$ for $l \neq 1$ where $\mathbf{0}$ is a zero vector and $\tilde{q} = (q, \alpha)$. Then the value of D at each point is

$$D(q, \alpha) = \begin{cases} M_w(d) \left(\kappa_{d-1} \left(\cdots M_w(1) \sqrt{B_X^2 + 1} \right) \right) & \text{if } q = q_1, \alpha = 1, \\ M_w(d) \left(\kappa_{d-1} \left(\cdots M_w(1) \frac{B_X^2}{\sqrt{B_X^2 + 1}} \right) \right) & \text{if } q = q_1, \alpha = 0, \\ M_w(d) \left(\kappa_{d-1} \left(\cdots M_w(1) \frac{1 - B_X^2}{\sqrt{B_X^2 + 1}} \right) \right) & \text{if } q = -q_1, \alpha = 1, \\ M_w(d) \left(\kappa_{d-1} \left(\cdots M_w(1) \frac{-B_X^2}{\sqrt{B_X^2 + 1}} \right) \right) & \text{if } q = -q_1, \alpha = 0. \end{cases}$$

For $0 \leq i \leq j \leq 2$, the neural distance d is described as follows,

$$\begin{aligned} d(p_i, p_j) &= \sup_D |\mathbf{E}_{p_i} D(Q^\alpha, \alpha) - \mathbf{E}_{p_j} D(Q^\alpha, \alpha)| \\ &= (j - i) \delta_{q,a} |(D(q_1, 1) - D(-q_1, 1)) + (D(q_1, 0) - D(-q_1, 0))|, \\ &\geq \delta_{q,a} |(D(q_1, 1) + D(q_1, 0)) - (D(-q_1, 0) + D(-q_1, 1))|, \end{aligned}$$

On the basis of the distribution, we set $\delta = \log(2)/(80\sqrt{n}) < 0.005$.

$$\begin{aligned}
n\text{KL}(p_i||p_0) &= 2n \left(\frac{1}{4} - i\delta\right) \log(1 - 4i\delta) + 2n \left(\frac{1}{4} + i\delta\right) \log(1 + 4i\delta), \\
&= \frac{n}{2} \log(1 - 4^2 i^2 \delta^2) + 2ni\delta \log\left(1 + \frac{8i\delta}{1 - 4i\delta}\right), \\
&\leq n4^2 i^2 \delta^2 \left(\frac{1}{2} \times \frac{1 + 4i\delta}{1 - 4i\delta}\right), \\
&\leq n4^2 i^2 \delta^2,
\end{aligned}$$

so we have

$$\frac{1}{2} \sum_{i=1}^2 n\text{KL}(p_i||p_0) \leq 80n\delta^2 \leq \frac{\log(2)}{80} \log(2).$$

Hence, by Fano's lemma, we obtain

$$\inf_{\hat{p}_n} \sup_{p_{Q^\alpha, \alpha} \in \mathcal{P}_{Q^\alpha, \alpha}} P[d(p_{Q^\alpha, \alpha}, \hat{p}_n)] \geq \frac{\sqrt{2}}{1 + \sqrt{2}} \left(\frac{39}{40} - \frac{\log(4)}{40}\right) > 0.55.$$

B.7 Proposition 3

Let's denote $W_1 = [W_{1,1}, W_{1,2}]$ with $W_{1,1} \in \mathbb{R}^{p_1}$, $W_{1,2} \in \mathbb{R}$. The derivative w.r.t. $W_{1,1}$ can be expressed as

$$\frac{\partial \hat{L}_b^\alpha(D^{(t)}, G^{(t)})}{\partial W_{1,1}} = \frac{1}{n_b} \sum_{i=1}^{n_b} Q_i^{\alpha_i} - \frac{1}{m_b} \sum_{j=1}^{m_b} G^{(t)}(Z_j^{\alpha_j}, \alpha_j).$$

By the iterative rule of the covariance,

$$\begin{aligned}
\text{Cov}(Q_i^{\alpha_i}) &= \mathbf{E}(\text{Cov}(Q_i^{\alpha_i} | \alpha_i)) + \text{Cov}(\mathbf{E}(Q_i^{\alpha_i} | \alpha_i)), \\
&= \mathbf{E}(\alpha_i^2 + (1 - \alpha_i)^2 \text{Cov}(X_1)).
\end{aligned}$$

Since α_i follows the distribution of (7),

$$\begin{aligned}
\mathbf{E}(\alpha_i^2 + (1 - \alpha_i)^2) &= r(\alpha_0^2 + (1 - \alpha_0)^2) + (1 - r)\mathbf{E}(\alpha_i^2), \\
&= \frac{2}{3} + \frac{r}{3}, \quad \because \alpha_0 = 1.
\end{aligned}$$

By the assumption of the generator, we also obtain $\text{Cov}(G(Z^{\alpha_i})) = \mathbf{E}(\alpha_i^2 + (1 - \alpha_i)^2 \text{Cov}(G(Z_1, 1)))$

$$\text{Cov}\left(\frac{\partial \hat{L}_b^\alpha(D^{(t)}, G^{(t)})}{\partial W_{1,1}}\right) = \left(\frac{2}{3} + \frac{r}{3}\right) \left(\frac{\text{Cov}(X_1)}{n_b} + \frac{\text{Cov}(G(Z_1, 1))}{m_b}\right).$$

For the single parameter $W_{1,2}$, the derivative is

$$\frac{\partial \hat{L}_b^\alpha(D^{(t)}, G^{(t)})}{\partial W_{1,2}} = \frac{1}{n_b} \sum_{i=1}^{n_b} \alpha_i - \frac{1}{m_b} \sum_{j=1}^{m_b} \alpha_j,$$

and its variance is

$$\text{Var}\left(\frac{\partial \hat{L}_b^\alpha(D^{(t)}, G^{(t)})}{\partial W_{1,2}}\right) = \frac{\text{Var}(\alpha_i)}{n_b} + \frac{\text{Var}(\alpha_j)}{m_b} \leq \frac{1}{4} \left(\frac{1}{n_b} + \frac{1}{m_b}\right),$$

where $0 \leq \text{Var}(\alpha_i) \leq \frac{1}{4}$. Note the minimum is found at $r = 1$, and the maximum comes from $\alpha_i \sim \text{Ber}(\frac{1}{2})$. On the other hand, the counterpart gradient's variance is

$$\text{tr}\left(\text{Cov}\left(\frac{\partial \hat{L}_b^1(D^{(t)}, G^{(t)})}{\partial W_1}\right)\right) = \left(\frac{\text{Cov}(X_1)}{n_b} + \frac{\text{Cov}(G(Z_1, 1))}{m_b}\right).$$

Therefore, we see the condition to satisfy

$$\begin{aligned} \left(\frac{\text{tr}(\text{Cov}(X_1))}{n_b} + \frac{\text{tr}(\text{Cov}(G(Z_1, 1)))}{m_b}\right) &\geq \left(\frac{2}{3} + \frac{r}{3}\right) \left(\frac{\text{tr}(\text{Cov}(X_1))}{n_b} + \frac{\text{tr}(\text{Cov}(G(Z_1, 1)))}{m_b}\right) \\ &\quad + \text{Var}(\alpha_1) \left(\frac{1}{n_b} + \frac{1}{m_b}\right). \end{aligned}$$

C Algorithm

Algorithm 1 describes the PT+CP implementation (PTGAN), and Algorithms 2 and 3 implement FairPTGAN.

Algorithm 1: Parallely Tempered Generative Adversarial Nets

Data: $\{x_i\}_{i=1}^n$ be a set of training data set. Set the training iteration T and for the inner loop T' , the minibatch size $n_b = m_b$, $t = 0$, the penalty size λ , the ratio r , the learning rate γ_D and γ_G , and initialize $\mathbf{w}^{(0)}$ and $\mathbf{v}^{(0)}$.

Result: $\mathbf{v}^{(T)}$

while $t \leq T$ **do**

Set $t' = 0$ and $t = t + 1$

Randomly choose $\{x_{(i)}\}_{i=1}^{n_b}$ and $\{x'_{(i)}\}_{i=1}^{n_b}$ from $\{x_i\}_{i=1}^n$ independently.

Generate $\{z_{(i)}\}_{i=1}^{n_b}$ and $\{z'_{(i)}\}_{i=1}^{n_b}$ from p_Z , $\{\alpha_{(i)}^{(1)}\}_{i=1}^{n_b} \sim p_\alpha$, $\{\alpha_{(i)}^{(2)}\}_{i=1}^{n_b} \sim \text{Unif}(0, 1)$, and $\{\nu_{(i)}\}_{i=1}^{n_b} \sim \text{Unif}(0, 1)$.

Create $\{q_{(i)}^{(1)} = \alpha_{(i)}^{(1)}x_{(i)} + (1 - \alpha_{(i)}^{(1)})x'_{(i)}\}_{i=1}^{n_b}$, $\{q_{(i)}^{(2)} = \alpha_{(i)}^{(2)}x_{(i)} + (1 - \alpha_{(i)}^{(2)})x'_{(i)}\}_{i=1}^{n_b}$,

$\{\tilde{q}_{(i)} = \nu_{(i)}q_{(i)}^{(1)} + (1 - \nu_{(i)})q_{(i)}^{(2)}\}_{i=1}^{n_b}$, $\{z_{(i)}^{(1)} = \alpha_{(i)}^{(1)}z_{(i)} + (1 - \alpha_{(i)}^{(1)})z'_{(i)}\}_{i=1}^{n_b}$, and

$\{\tilde{\alpha}_{(i)} = \nu_{(i)}\alpha_{(i)}^{(1)} + (1 - \nu_{(i)})\alpha_{(i)}^{(2)}\}_{i=1}^{n_b}$.

while $t' \leq T'$ **do**

$t' = t' + 1$

$$\hat{L}_b(\mathbf{w}^{(t)}, \mathbf{v}^{(t)}) = \frac{1}{n_b} \sum_{i=1}^{n_b} D_{\mathbf{w}^{(t)}}(q_{(i)}^{(1)}, \alpha_{(i)}^{(1)}) - D_{\mathbf{w}^{(t)}}(G_{\mathbf{v}^{(t)}}(z_{(i)}^{(1)}, \alpha_{(i)}^{(1)}), \alpha_{(i)}^{(1)})$$

$$\hat{H}(\mathbf{w}^{(t)}) = \frac{1}{n_b} \sum_{i=1}^{n_b} \left(\nabla_{\tilde{q}_i} D_{\mathbf{w}^{(t)}}(\tilde{q}_i, \tilde{\alpha}_{(i)}) \cdot (q_{(i)}^{(1)} - q_{(i)}^{(2)}) \right)^2$$

$$\mathbf{w}^{(t+1)} = \mathbf{w}^{(t)} + \gamma_D \frac{\partial}{\partial \mathbf{w}^{(t)}} \left(\hat{L}_b(\mathbf{w}^{(t)}, \mathbf{v}^{(t)}) - \lambda \hat{H}(\mathbf{w}^{(t)}) \right)$$

end

$$\hat{L}_b^G(\mathbf{w}^{(t+1)}, \mathbf{v}^{(t)}) = -\frac{1}{n_b} \sum_{i=1}^{n_b} D_{\mathbf{w}^{(t+1)}}(G_{\mathbf{v}^{(t)}}(z_{(i)}^{(1)}, \alpha_{(i)}^{(1)}), \alpha_{(i)}^{(1)})$$

$$\mathbf{v}^{(t+1)} = \mathbf{v}^{(t)} - \gamma_G \frac{\partial}{\partial \mathbf{v}^{(t)}} \hat{L}_b^G(\mathbf{w}^{(t+1)}, \mathbf{v}^{(t)})$$

end

Algorithm 2: Minibatch Construction (MC) for FairPTGAN

Data: $\{x_i^{(0)}\}_{i=1}^{n_0}$ and $\{x_i^{(1)}\}_{i=1}^{n_1}$ are the sets of either $A = 0$ or $A = 1$. The subscript

(i) denotes the i th randomly selected sample. Let $n'_b = n_b/2$.

Result: $\{q_{(i)}^{(1)}\}_{i=1}^{n_b}$, $\{q_{(i)}^{(2)}\}_{i=1}^{n_b}$, $\{\tilde{q}_{(i)}\}_{i=1}^{n_b}$, $\{z_{(i)}^{(1)}\}_{i=1}^{n_b}$, $\{\alpha_{(i)}^{(1)}\}_{i=1}^{n_b}$, and $\{\tilde{\alpha}_{(i)}\}_{i=1}^{n_b}$.

Randomly choose $\{x_{(i)}^{(0)}\}_{i=1}^{n'_b}$ from $\{x_i^{(0)}\}_{i=1}^{n_0}$ and $\{x'_{(i)}{}^{(0)}\}_{i=1}^{n'_b}$ from $\{x_i^{(0)}\}_{i=1}^{n_0} \setminus \{x_{(i)}^{(0)}\}_{i=1}^{n'_b}$.

Randomly choose $\{x_{(i)}^{(1)}\}_{i=1}^{n'_b}$ from $\{x_i^{(1)}\}_{i=1}^{n_1}$ and $\{x'_{(i)}{}^{(1)}\}_{i=1}^{n'_b}$ from $\{x_i^{(1)}\}_{i=1}^{n_1} \setminus \{x_{(i)}^{(1)}\}_{i=1}^{n'_b}$.

Randomly choose $\{z_{(i)}\}_{i=1}^{n_b}$ and $\{z'_{(i)}\}_{i=1}^{n_b}$ from p_Z .

Generate $\{\alpha_{(i)}^{(1)}\}_{i=1}^{n'_b} \sim p_\alpha$, $\{\alpha_{(i)}^{(2)}\}_{i=1}^{n'_b} \sim \text{Unif}(0, 1)$, and $\{\nu_{(i)}\}_{i=1}^{n'_b} \sim \text{Unif}(0, 1)$.

Create $\{\tilde{x}_{(i)}^{(1)} = \alpha_{(i)}^{(1)}x_{(i)}^{(0)} + (1 - \alpha_{(i)}^{(1)})x'_{(i)}{}^{(0)}\}_{i=1}^{n'_b}$ and $\{\tilde{x}_{(i)}^{(2)} = (1 - \alpha_{(i)}^{(1)})x_{(i)}^{(0)} + \alpha_{(i)}^{(1)}x'_{(i)}{}^{(0)}\}_{i=1}^{n'_b}$.

Create $\{\hat{x}_{(i)}^{(1)} = \alpha_{(i)}^{(2)}x'_{(i)}{}^{(0)} + (1 - \alpha_{(i)}^{(2)})x_{(i)}^{(1)}\}_{i=1}^{n'_b}$ and $\{\hat{x}_{(i)}^{(2)} = (1 - \alpha_{(i)}^{(2)})x'_{(i)}{}^{(0)} + \alpha_{(i)}^{(2)}x_{(i)}^{(1)}\}_{i=1}^{n'_b}$.

Produce $\{q_{(i)}^{(1)}\}_{i=1}^{n_b} = \{\tilde{x}_{(i)}^{(1)}\}_{i=1}^{n'_b} \cup \{\tilde{x}_{(i)}^{(2)}\}_{i=1}^{n'_b}$, $\{q_{(i)}^{(2)}\}_{i=1}^{n_b} = \{\hat{x}_{(i)}^{(1)}\}_{i=1}^{n'_b} \cup \{\hat{x}_{(i)}^{(2)}\}_{i=1}^{n'_b}$,

$\{\tilde{q}_{(i)} = \nu_{(i)}q_{(i)}^{(1)} + (1 - \nu_{(i)})q_{(i)}^{(2)}\}_{i=1}^{n_b}$, $\{z_{(i)}^{(1)} = \alpha_{(i)}^{(1)}z_{(i)} + (1 - \alpha_{(i)}^{(1)})z'_{(i)}\}_{i=1}^{n_b}$, and

$\{\tilde{\alpha}_{(i)} = \nu_{(i)}\alpha_{(i)}^{(1)} + (1 - \nu_{(i)})\alpha_{(i)}^{(2)}\}_{i=1}^{n_b}$.

Algorithm 3: Fair Parallely Tempered Generative Adversarial Nets

Data: $\{x_i\}_{i=1}^n$ be a set of training data set. Set the training iteration T and for the inner loop T' , the minibatch size $n_b = m_b$, $t = 0$, the penalty size λ , the ratio r , the learning rate γ_D and γ_G , and initialize $\mathbf{w}^{(0)}$ and $\mathbf{v}^{(0)}$.

Result: $\mathbf{v}^{(T)}$

while $t \leq T$ **do**

$t = t + 1$

$$\begin{aligned} & \{q_{(i)}^{(1)}\}_{i=1}^{n_b}, \{q_{(i)}^{(2)}\}_{i=1}^{n_b}, \{\tilde{q}_{(i)}\}_{i=1}^{n_b}, \{z_{(i)}^{(1)}\}_{i=1}^{n_b}, \{\alpha_{(i)}^{(1)}\}_{i=1}^{n_b}, \{\tilde{\alpha}_{(i)}\}_{i=1}^{n_b} \\ & = \text{MC}(\{x_i^{(0)}\}_{i=1}^{n_0}, \{x_i^{(1)}\}_{i=1}^{n_1}) \end{aligned}$$

 Set $t' = 0$.

while $t' \leq T'$ **do**

$t' = t' + 1$

$$\hat{L}_b(\mathbf{w}^{(t)}, \mathbf{v}^{(t)}) = \frac{1}{n_b} \sum_{i=1}^{n_b} D_{\mathbf{w}^{(t)}}(q_{(i)}^{(1)}, \alpha_{(i)}^{(1)}) - D_{\mathbf{w}^{(t)}}(G_{\mathbf{v}^{(t)}}(z_{(i)}^{(1)}, \alpha_{(i)}^{(1)}), \alpha_{(i)}^{(1)})$$

$$\hat{H}(\mathbf{w}^{(t)}) = \frac{1}{n_b} \sum_{i=1}^{n_b} \left(\nabla_{\tilde{q}_i} D_{\mathbf{w}^{(t)}}(\tilde{q}_i, \tilde{\alpha}_{(i)}) \cdot (q_{(i)}^{(1)} - q_{(i)}^{(2)}) \right)^2$$

$$\mathbf{w}^{(t+1)} = \mathbf{w}^{(t)} + \gamma_D \frac{\partial}{\partial \mathbf{w}^{(t)}} \left(\hat{L}_b(\mathbf{w}^{(t)}, \mathbf{v}^{(t)}) - \lambda \hat{H}(\mathbf{w}^{(t)}) \right)$$

end

$$\hat{L}_b^G(\mathbf{w}^{(t+1)}, \mathbf{v}^{(t)}) = -\frac{1}{n_b} \sum_{i=1}^{n_b} D_{\mathbf{w}^{(t+1)}}(G_{\mathbf{v}^{(t)}}(z_{(i)}^{(1)}, \alpha_{(i)}^{(1)}), \alpha_{(i)}^{(1)})$$

$$\mathbf{v}^{(t+1)} = \mathbf{v}^{(t)} - \gamma_G \frac{\partial}{\partial \mathbf{v}^{(t)}} \hat{L}_b^G(\mathbf{w}^{(t+1)}, \mathbf{v}^{(t)})$$

end

D Simulation

D.1 Details of Figure 2

Proposition 2 and Theorem 1 imply that the size of weight matrices should be appropriately controlled to calculate the gradients’ variance. In every iteration, therefore, $D^{(t)}$ is trained with the penalty of Mescheder et al. (2018). Since $G^{(t)}$ is fixed to generate the left mode, it does not need to be updated. After the one-step update of D , $\partial \hat{L}_b^i / \partial \mathbf{w}^{(t)}$ is found for all $i = 1, \dots, n_b$ where $\hat{L}_b^i = D(X_i) - G(Z_i)$, so that there are n_b number of gradient for every single element in $\mathbf{w}^{(t)}$. Then the variance is calculated elementwisely and summed up all.

D.2 Details in Section 5.1

D.2.1 Image data generation

Evaluation metrics Inception Score (IS, Salimans et al., 2016) and Fréchet Inception Distance (FID, Heusel et al., 2017) scores are calculated based on InceptionV3 (Szegedy et al., 2015) which is a pre-trained classifier on **ImageNet**. Let $p(y|x)$ be the classifier and denote by $\tilde{y}(x)$ the intermediate output after the global max-pooling layer in the classifier where labels and images match y and x respectively. The scores are calculated as follows:

$$\begin{aligned} \text{IS} &= \exp \left(\mathbf{E}_{X \sim p_G(Z)} (\text{KL}(p(y|X) || p(y))) \right), \\ \text{FID} &= \|\mu_X - \mu_G\|_2^2 + \text{tr} \left(\Sigma_X + \Sigma_G - 2 \left(\Sigma_X^{\frac{1}{2}} \Sigma_G \Sigma_X^{\frac{1}{2}} \right)^{\frac{1}{2}} \right), \end{aligned}$$

where $\mu_X = \mathbf{E}(\tilde{y}(X))$, $\mu_G = \mathbf{E}(\tilde{y}(G(Z)))$, $\Sigma_X = \text{Cov}(\tilde{y}(X))$, and $\Sigma_G = \text{Cov}(\tilde{y}(G(Z)))$. For IS, the lower the entropy of $p(y|G(Z))$ is, the higher fidelity images G produces. The marginal probability $p(y) = \int p(y|G(z))p(G(z))p(z)dz$ having higher entropy implies more diversity. Therefore, as the discrepancy of the KL divergence increases, it can be said that the generator achieves higher performance on both the high quality of images and

the diversity. On the one hand, FID measures the distance in the latent space under the assumption that the latent feature follows multivariate Gaussian distributions.

Simulation setup Simulation settings in Section 5.1 for CIFAR10 and TinyImageNet are present here. The network architectures of D and G follow the CNN-based structure (Table 4) used in the spectral normalization GAN training (Miyato et al., 2018). A convolutional layer with 3×3 kernel, 1 stride, and 64 filters is denoted as [conv: 3×3 , 1, 64], and a deconvolutional layer is also written in the same way. For p_x , CIFAR10 and TinyImageNet have 32 and 64. The total number of iterations T is set to 100k and 62k with minibatches having 100 and 64 data instances for each data set. Referring to Zhou et al. (2019), the Adam optimizer’s hyperparameters are set to $\beta_1 = 0.0$ and $\beta_2 = 0.9$ with the learning rates for D and G as 0.0001 (Kingma and Ba, 2015). The spectral normalization layer (SN) is only applied to the original competitor Miyato et al. (2018). The penalty parameters for λ_{MP} (MP, Zhou et al., 2019) and λ_{GP} (GP, Gulrajani et al., 2017) are specified as $\lambda_{\text{MP}} = 1$ and $\lambda_{\text{GP}} = 10$ by referring to their works. For LN (Jenni and Favaro, 2019), the noise generator has the same structure as the image generator by referring to their work. IS/FID scores are measured at 5 different t points that equally space the total number of iterations T since the evaluation of IS and FID is computationally heavy. The best score is determined from those.

Other GAN metrics Our simulation study further considers the popular GAN metrics such as the Jensen-Shannon divergence (JSD) and the Pearson χ^2 divergence (PD). In our

$X \in \mathbb{R}^{p_x \times p_x \times 3}$	$Z \in \mathbb{R}^{128}$
[conv: 3×3 , 1, 64] (SN) lReLU(0.2)	dense $\rightarrow 6 \times 6 \times 512$
[conv: 4×4 , 1, 64] (SN) lReLU(0.2)	[deconv: 4×4, 2, 256] BN ReLU
[conv: 3×3, 1, 128] (SN) lReLU(0.2)	[deconv: 4×4, 2, 128] BN ReLU
[conv: 4×4, 1, 128] (SN) lReLU(0.2)	[deconv: 4×4, 2, 64] BN ReLU
[conv: 3×3, 1, 256] (SN) lReLU(0.2)	reshape $p_x \times p_x \times 3$
[conv: 4×4, 1, 256] (SN) lReLU(0.2)	
[conv: 3×3, 1, 512] (SN) lReLU(0.2)	
dense $\rightarrow 1$	(b) Generator

(a) Critic

Table 4: Convolutional neural network structures for D and G in CIFAR10 $p_x = 32$ and TinyImageNet $p_x = 64$.

notations, their loss functions are written as:

$$\text{JSD} = \sup_D \mathbf{E}(\log D(X)) + \mathbf{E}(\log(1 - D(G(Z)))) ,$$

$$\text{PD} = \sup_D \frac{1}{2} \mathbf{E}_X ((D(X) - 1)^2) + \frac{1}{2} \mathbf{E}_Z (D(G(Z))^2) .$$

To see more details, refer to the original works.

Penalty-based GAN training The Lipschitz GAN (Zhou et al., 2019) uses the maximum penalty is defined as $\text{MP} = \lambda_{\text{MP}} \max_i \|\nabla_{\tilde{X}_i} D(\tilde{X}_i)\|^2$ where $\tilde{X}_i = \nu X_i + (1 - \nu)G(Z_i)$ where ν is randomly drawn from $\text{Unif}(0, 1)$. The Wasserstein GAN with the gradient penalty uses $\text{GP} = \lambda_{\text{GP}} \mathbf{E}((\|\nabla_{\tilde{X}} D(\tilde{X}_i)\| - 1)^2)$ where \tilde{X}_i is the random interpolation as MP.

Additional results While we use the penalty parameter for MP and GP recommended in their papers, we find extra results with the different parameters of λ_{MP} and λ_{GP} . Due to the limited computation resources, the results are only based on the neural distance, and they are shown in Table 5. Table 6 justifies the high value of r because of the bias-variance trade-off. It highlights that the performance is worse when no interpolation points are used.

Table 5: Summary of IS/FID in CIFAR10 and TinyImageNet for MP and GP. Standard deviations are averaged across 10 independent implementations. All values are rounded to the third decimal place.

		CIFAR10		TinyImageNet	
$d_{\mathcal{D}}$	Type	IS (\uparrow)	FID (\downarrow)	IS (\uparrow)	FID (\downarrow)
ND	MP ($\lambda_{\text{MP}} = 10$)	6.833 (0.090)	30.048 (0.979)	7.210 (0.107)	105.358 (1.889)
	MP ($\lambda_{\text{MP}} = 100$)	6.722 (0.054)	30.569 (0.457)	7.257 (0.215)	105.613 (0.737)
	GP ($\lambda_{\text{GP}} = 1$)	6.773 (0.145)	29.903 (0.973)	7.143 (0.210)	106.596 (1.811)
	GP ($\lambda_{\text{GP}} = 100$)	6.759 (0.090)	29.545 (0.592)	7.124 (0.164)	106.495 (1.711)

Table 6: Comparison by differing the hyperparameter r for the neural distance

		CIFAR10		TinyImageNet	
		$r = 1.0$	$r = 0.9$	$r = 1.0$	$r = 0.9$
IS		6.885 (0.145)	7.248 (0.067)	7.384 (0.173)	7.508 (0.224)
FID		28.551 (2.028)	25.087 (0.962)	102.161 (2.592)	102.934 (2.194)

D.2.2 Tabular data generation

Data description All models are tested on the following benchmark data sets:

- **Adult** is for predicting whether an individual’s annual income is greater than \$50K or not. The data consists of 32561 individuals with 15 variables, but we exclude ‘education’ and ‘fnlwtg’ by referring to the pre-processing step in Cho et al. (2020). For more details about data, refer to <https://archive.ics.uci.edu/ml/datasets/adult>.
- **Law School Admission** consists of 124557 individuals with 15 variables. Considering the duplication of columns and rows, we select ‘LSAT’, ‘GPA’, ‘Gender’, ‘Race’, and ‘resident’. The task is to predict whether an applicant receives admission. For more details about data, refer to Wightman (1998).
- **Credit Card Default** is for predicting whether or not a customer declares default. This data set includes 30000 individuals with 25 variables. We only drop ‘ID’ in the simulation study. For more details about data, refer to <https://archive.ics.uci.edu/dataset/350/default+of+credit+card+clients>.

In all data sets, continuous variables are scaled such that they are within $[-1, 1]$. Discrete variables are transformed to one-hot encoding.

Simulation setup The network architectures of D and G are based on the dense layers as shown in Table 7. The generator consists of two parts to put different activation functions for continuous and discrete variables. The continuous variables are generated through [common]-[continuous] while each one-hot encoded discrete variable is individually generated through [common]-[discrete]. The final layer in [discrete] employs the Gumbel-softmax function (Jang et al., 2017) that enables the one-hot encoding procedure to be differentiable. The notations d_X , $d_{\text{continuous}}$, and d_{discrete} are generic to denote the dimension of input space, the number of continuous variables, and the total number of discrete variables each of which is one-hot encoded. For each model, we implement 10 experiments with 200 epochs for

Adult and Credit Card Default but 40 epochs for Law School Admission while they all have the 100 minibatch size. The Adam optimizer is set to be the same as used in the image generation tasks. For the data sets, the total number of iterations of T is approximately 57k, 35k, and 53k for Adult, Law School Admission, and Credit Card Default. The evaluation of S_t is made at 50 equally spaced points in $\{0, \dots, T\}$.

$X \in \mathbb{R}^{d_x}$	$Z \in \mathbb{R}^{16}$
dense 64 ReLU \times 7	[common] dense 64 BN ReLU \times 7
dense \rightarrow 1	[continuous] dense $d_{\text{continuous}}$
(a) Critic	[discrete] dense Gumbel-softmax d_{discrete}
	(b) Generator

Table 7: Dense neural network structures for D and G .

Additional results We find further results of MP by differing the penalty parameter λ_{MP} . Table 9 also shows that ours defeats the Lipschitz GAN model. For the consistent use of the parameter, the results of $\lambda_{\text{MP}} = 1$ appear in the main text.

D.3 Details in Section 5.2

Evaluation metric A Pareto frontier is a set of solutions that are not dominated by other pairs. For example, $(0.7, 0.7)$, a pair of AUC and SP, is dominated by $(0.8, 0.4)$ but not by $(0.6, 0.6)$. To see more details, refer to Emmerich and Deutz (2018).

Implementation of FairPTGAN The proposed FairPTGAN model first yields mini-batches from Algorithm 2 and then implements Algorithm 3 to learn D and G .

Table 8: Summary of \mathcal{S}_T : all scores appearing below are the average of 10 replicated implementations. The standard deviation appears in the parenthesis.

Data	$d_{\mathcal{D}}$	Type	RF (\downarrow)	SVM (\downarrow)	LR (\downarrow)
Adult	JSD	PT + CP	0.022 (0.004)	0.037 (0.004)	0.028 (0.003)
		MP	0.059 (0.019)	0.069 (0.022)	0.058 (0.019)
	PD	PT + CP	0.023 (0.003)	0.039 (0.007)	0.026 (0.004)
		MP	0.047 (0.021)	0.054 (0.011)	0.044 (0.011)
Law School.	JSD	PT + CP	0.020 (0.014)	0.023 (0.009)	0.008 (0.006)
		MP	0.093 (0.022)	0.101 (0.022)	0.068 (0.024)
	PD	PT + CP	0.019 (0.007)	0.020 (0.004)	0.006 (0.001)
		MP	0.096 (0.017)	0.099 (0.018)	0.069 (0.016)
Credit Card.	JSD	PT + CP	0.052 (0.009)	0.061 (0.017)	0.036 (0.008)
		MP	0.147 (0.021)	0.164 (0.038)	0.146 (0.030)
	PD	PT + CP	0.050 (0.009)	0.046 (0.012)	0.035 (0.010)
		MP	0.126 (0.040)	0.138 (0.047)	0.122 (0.043)

FairWGANP and GeoRepair Rajabi and Garibay (2022) suggested two-step learning procedure: 1) training $G^{(t)}$ up to T iteration using WGANP (Gulrajani et al., 2017) and then 2) regularizing $G^{(T+l)}(Z)$, for $l = 1, \dots, T'$, with the fairness penalty formulated as $\lambda_f |\mathbf{E}(\tilde{Y}|\tilde{A} = 1) - \mathbf{E}(\tilde{Y}|\tilde{A} = 0)|$ where $(\tilde{C}, \tilde{A}, \tilde{Y}) \sim G^{(T+l)}(Z)$. Thus, λ_f controls the trade-off, and it is set to $\lambda_f = 10$ by referring to Rajabi and Garibay (2022). In Feldman et al. (2015), the authors proposed the geometric repair that transforms a univariate covariate c to $(1 - \lambda_p)F_a^{-1}(q) + \lambda_p F_A^{-1}(q)$ where $F_a(x)$ is the conditional cumulative distribution of c given $a \in \{0, 1\}$ and $F_A^{-1}(q) = \text{median}_{a \in \{0, 1\}} F_a^{-1}(q)$ with $q = F_a(c)$. In our study, this pre-processing step is applied to the FairPTGAN model with $\alpha = 1$ with 5 equally spaced $\lambda_p \in [0, 1]$ considered.

Table 9: Summary of S_T of MP: all scores appearing below are the average of 10 replicated implementations. The standard deviation appears in the parenthesis.

Data	$d_{\mathcal{D}}$	Type	RF	SVM	LR
Adult	JSD	MP ($\lambda_{MP} = 10$)	0.028 (0.014)	0.043 (0.019)	0.034 (0.015)
		MP ($\lambda_{MP} = 100$)	0.030 (0.016)	0.044 (0.010)	0.034 (0.012)
	PD	MP ($\lambda_{MP} = 10$)	0.043 (0.024)	0.051 (0.018)	0.041 (0.020)
		MP ($\lambda_{MP} = 100$)	0.035 (0.025)	0.045 (0.015)	0.034 (0.013)
	ND	MP ($\lambda_{MP} = 10$)	0.043 (0.025)	0.047 (0.016)	0.039 (0.013)
		MP ($\lambda_{MP} = 100$)	0.025 (0.014)	0.042 (0.016)	0.032 (0.012)
Law School.	JSD	MP ($\lambda_{MP} = 10$)	0.092 (0.023)	0.095 (0.024)	0.063 (0.025)
		MP ($\lambda_{MP} = 100$)	0.064 (0.032)	0.065 (0.027)	0.038 (0.026)
	PD	MP ($\lambda_{MP} = 10$)	0.079 (0.023)	0.080 (0.026)	0.057 (0.029)
		MP ($\lambda_{MP} = 100$)	0.059 (0.035)	0.060 (0.033)	0.037 (0.023)
	ND	MP ($\lambda_{MP} = 10$)	0.079 (0.020)	0.084 (0.022)	0.056 (0.018)
		MP ($\lambda_{MP} = 100$)	0.063 (0.027)	0.066 (0.030)	0.039 (0.027)
Credit Card.	JSD	MP ($\lambda_{MP} = 10$)	0.121 (0.051)	0.126 (0.055)	0.113 (0.058)
		MP ($\lambda_{MP} = 100$)	0.134 (0.041)	0.153 (0.035)	0.132 (0.042)
	PD	MP ($\lambda_{MP} = 10$)	0.121 (0.057)	0.127 (0.058)	0.114 (0.061)
		MP ($\lambda_{MP} = 100$)	0.147 (0.020)	0.170 (0.023)	0.154 (0.031)
	ND	MP ($\lambda_{MP} = 10$)	0.128 (0.045)	0.136 (0.042)	0.121 (0.040)
		MP ($\lambda_{MP} = 100$)	0.150 (0.021)	0.174 (0.039)	0.150 (0.023)

Simulation setup The study particularly considers Adult and Law School Admission data sets showing evident discrimination impact on prediction tasks. For Adult, the “race” variable is specified as a sensitive attribute that is binarized to be white and non-white. Similarly in Law School Admission, the “White” variable is used as a sensitive attribute while “Race” is dropped. For a fair comparison, the total number of iterations for both

FairPTGAN and FairWGANGP is specified as $T = 100k$ but FairWGANGP has extra $T/2$ iterations for its second training phase with $\lambda_f = 10$. As mentioned, GeoRepair is implemented to the produced data set by FairPTGAN models with $\alpha = 1$. For PTGAN, r is set to 0.2. In all cases, the minibatch size is specified as 200. Other configurations are the same with Section D.2.2. To draw smooth Pareto-frontier curves, each run produces 20 independent data sets with the last iterate of the generator, i.e., $G^{(100k)}$ for FairPTGAN and $G^{(150k)}$ for FairWGANGP. Thus, 200 independent sets from the 10 independent runs are used to draw the results.

Additional results Similar to Table 3 in the main text, we draw Table 10 with different thresholds. It is noteworthy that FairPTGAN captures smoother trade-off curves than the two competitors. GeoRepair and FairWGANGP in Table 10 have the same scores, especially in LR with Table 3.

Table 10: Averages of the 10 smallest SP scores whose AUCs are greater than the thresholds (≥ 0.70 for Adult and ≥ 0.70 for Law School). Standard deviations are in the parentheses next to the averages.

Data	Model	RF (\downarrow)	SVM (\downarrow)	LR (\downarrow)
Adult	FairPTGAN	0.008 (0.004)	0.015 (0.009)	0.058 (0.012)
	FairWGANGP	0.051 (0.009)	0.075 (0.006)	0.080 (0.005)
	GeoRepair	0.069 (0.007)	0.039 (0.019)	0.098 (0.012)
Law School.	FairPTGAN	0.111 (0.018)	0.107 (0.008)	0.137 (0.014)
	FairWGANGP	0.147 (0.007)	0.120 (0.005)	0.175 (0.003)
	GeoRepair	0.119 (0.019)	0.144 (0.004)	0.182 (0.003)

Supplementary References

- Chhachhi, S. and Teng, F. (2023). On the 1-wasserstein distance between location-scale distributions and the effect of differential privacy. *arXiv preprint arXiv:2304.14869*.
- Cho, J., Hwang, G., and Suh, C. (2020). A fair classifier using kernel density estimation. In *Advances in Neural Information Processing Systems 33*.
- Dowson, D. and Landau, B. (1982). The fréchet distance between multivariate normal distributions. *Journal of multivariate analysis*, 12(3):450–455.
- Emmerich, M. T. and Deutz, A. H. (2018). A tutorial on multiobjective optimization: fundamentals and evolutionary methods. *Natural computing*, 17:585–609.
- Feldman, M., Friedler, S. A., Moeller, J., Scheidegger, C., and Venkatasubramanian, S. (2015). Certifying and removing disparate impact. In *Proceedings of the 21th ACM SIGKDD International Conference on Knowledge Discovery and Data Mining*, pages 259–268. ACM.
- Golowich, N., Rakhlin, A., and Shamir, O. (2018). Size-independent sample complexity of neural networks. In *Conference On Learning Theory*, volume 75 of *Proceedings of Machine Learning Research*, pages 297–299. PMLR.
- Gulrajani, I., Ahmed, F., Arjovsky, M., Dumoulin, V., and Courville, A. C. (2017). Improved training of wasserstein gans. In *Advances in Neural Information Processing Systems*, volume 30. Curran Associates, Inc.
- Hendrycks, D., Mu, N., Cubuk, E. D., Zoph, B., Gilmer, J., and Lakshminarayanan, B. (2020). Augmix: A simple data processing method to improve robustness and uncer-

- tainty. In *Proceedings of the 8th International Conference on Learning Representations*. OpenReview.net.
- Heusel, M., Ramsauer, H., Unterthiner, T., Nessler, B., and Hochreiter, S. (2017). Gans trained by a two time-scale update rule converge to a local nash equilibrium. In *Advances in Neural Information Processing Systems 30*, pages 6626–6637.
- Jang, E., Gu, S., and Poole, B. (2017). Categorical reparameterization with gumbel-softmax. In *Proceedings of the 5th International Conference on Learning Representations*. OpenReview.net.
- Ji, K., Zhou, Y., and Liang, Y. (2021). Understanding estimation and generalization error of generative adversarial networks. *IEEE Trans. Inf. Theory*, 67(5):3114–3129.
- Kingma, D. P. and Ba, J. (2015). Adam: A method for stochastic optimization. In *Proceedings of the 3rd International Conference on Learning Representations*.
- Lu, Z., Pu, H., Wang, F., Hu, Z., and Wang, L. (2017). The expressive power of neural networks: A view from the width. In *Advances in Neural Information Processing Systems 30*, pages 6231–6239.
- Miyato, T., Kataoka, T., Koyama, M., and Yoshida, Y. (2018). Spectral normalization for generative adversarial networks. In *Proceedings of the 6th International Conference on Learning Representations*. OpenReview.net.
- Park, S., Yun, C., Lee, J., and Shin, J. (2021). Minimum width for universal approximation. In *Proceedings of the 9th International Conference on Learning Representations*. OpenReview.net.

- Rajabi, A. and Garibay, Ö. Ö. (2022). Tabfairgan: Fair tabular data generation with generative adversarial networks. *Mach. Learn. Knowl. Extr.*, 4(2):488–501.
- Salimans, T., Goodfellow, I. J., Zaremba, W., Cheung, V., Radford, A., and Chen, X. (2016). Improved techniques for training gans. In *Advances in Neural Information Processing Systems 29*, pages 2226–2234.
- Szegedy, C., Vanhoucke, V., Ioffe, S., Shlens, J., and Wojna, Z. (2015). Rethinking the inception architecture for computer vision. *CoRR*, abs/1512.00567.
- Verma, V., Lamb, A., Beckham, C., Najafi, A., Mitliagkas, I., Lopez-Paz, D., and Bengio, Y. (2019). Manifold mixup: Better representations by interpolating hidden states. In *Proceedings of the 36th International Conference on Machine Learning*, volume 97 of *Proceedings of Machine Learning Research*, pages 6438–6447. PMLR.
- Wightman, L. F. (1998). Lsac national longitudinal bar passage study. lsac research report series.
- Yun, S., Han, D., Chun, S., Oh, S. J., Yoo, Y., and Choe, J. (2019). Cutmix: Regularization strategy to train strong classifiers with localizable features. In *Proceedings of the IEEE/CVF international conference on computer vision*, pages 6022–6031. IEEE.
- Zhang, H., Cissé, M., Dauphin, Y. N., and Lopez-Paz, D. (2018). mixup: Beyond empirical risk minimization. In *Proceedings of the 6th International Conference on Learning Representations*. OpenReview.net.
- Zhou, Z., Liang, J., Song, Y., Yu, L., Wang, H., Zhang, W., Yu, Y., and Zhang, Z. (2019). Lipschitz generative adversarial nets. In *Proceedings of the 36th International Conference*

on Machine Learning, volume 97 of *Proceedings of Machine Learning Research*, pages 7584–7593. PMLR.